Phonon effects on the dynamics and fidelity of two-qubit gates using trapped Rydberg ions

Submitted May 29, 2022, in fulfillment of
the conditions for the award of the degree **MRes Physics.**

Phileo Aderiye
20316732

Supervised by Dr. Weibin Li

School of Physics and Astronomy University of Nottingham

Acknowledgements

I would like to thank Dr. Weibin Li for his supervision, without whose help this project couldn't have been completed. I would also like to thank Thomas Hamlyn and Thomas Antolin for their collaboration and discussions during the project, as well as Gary Mc-Cormack for his advice during the writing of this thesis.

Abstract

Ultra-cold Rydberg ions confined in a linear trap are presented as a possible solution to some of the major problems causing infidlities currently presented in quantum computing gates e.g. weak two-body interactions such as magnetic field fluctuations.

The dynamics and intrinsic fidelity of the controlled-Z gate are simulated using the Fock state $|gg, 00\rangle$ (where g and 0 denote the groundstates of the spin and phonon excitations respectively) of a two-qubit system, where the fidelity of the gate is found to be 0.9999472, satisfying the fidelity requirement for a scalable quantum computing gate of 0.9999.

The same was done for phonon coherent states of the form $|gg, \alpha, \alpha\rangle$, where the displacement operator takes the form $\mathcal{D}(\alpha) = \exp(\alpha a^\dagger - \alpha^\star a)$. It is shown, to obtain the fidelity needed for a reliable individual quantum gate of at least 0.97, the maximum value for alpha is $\alpha_{max} = 0.25$; to obtain the fidelity needed for a scalable quantum gate of at least 0.9999, the maximum value for alpha is $\alpha_{max} = 0.0525$.

Contents

List of Figures

Chapter 1

Introduction

On 19th February 1946, at a meeting of the *National Physics Laboratory* in Teddington, England, Alan Turing, a british mathematician and computer scientist, presented his now famous research proposal *'A Proposal for the Development in the Mathematics Division of an Automatic Computing Engine'* [4]. His landmark designs were derived mainly from the work he undertook at the Government Code & Cypher School (GC&SC) in Bletchely Park, Buckinghamshire, during the Second World War. Here he developed methods of breaking codes sent out by the Nazi military and their then famous *Enigma* machine. His work during this period of his life directly saved countless lives and resulted in a research proposal that contained designs for the world's first computer.

Since Turing's first proposal, computing has rapidly evolved. Modern computers, still based upon Turing's initial ideas, have far more computing power than early designs. However, despite the advancements in computing, there are still many problems computers (what will now be called *classical* computers) cannot solve.

For example, a classical computer is very good at multiplying large prime numbers, but extremely poor at factoring a large number into its primes [5]. This issue stems from the way in which a classical computer stores information; the information (be it a picture, document, or in this case a number) is converted into a string of *bits*, each bit either having a value of 0 or 1. Although this process is more involved for increasingly complex pieces of information, it is straightforward for a number as it can be converted directly from base 10 to base 2 and stored as binary.

As of the time of submission of this thesis, the lowest running time for the factorisation of a very large number into its primes can be achieved by the general number field sieve (GNFS) algorithm [6]. For a given b-bit number n (that is to say, a number 'n' which is 'b' bits long when converted into binary), the GNFS can factorise in time of the order $O(e^{1.9(\ln n)^{1/3}(\ln \ln n)^{2/3}})$.

When factorising very large numbers, this time becomes longer than the age of the universe which is clearly impractical to solve, and although it is not proven, it is expected that there cannot exist an algorithm, executable on a classical computer, that will be significantly better than the GNFS [7, 8], and produce a factorisation time of the order $O(b^k)$, where k is any positive integer. A new type of computation is needed.

The fundamental principle of quantum superposition can be used to build this new type of computer. This principle explains that a quantum state can be represented as the sum of two or more different quantum states, or conversely, one can "add" two or more quantum

states and the result will be an equally valid quantum state [9]. As opposed to a classical computer, the bits used to store information in this new type of computation are not limited to the absolute values of either 0 or 1, but because of quantum superposition, can be a combination of the states $|0\rangle$ and $|1\rangle$. These quantum bits are called *qubits*, and the new type of computer, a *quantum* computer. We can also use the fundamental principle of quantum entanglement to entanglement multiple qubits, as they are quantum systems. Using these two principles, we can make the quantum analogy of classical computing logic gates.

With a quantum computer, the factorisation of large numbers becomes much simpler with the use of an algorithm made specifically for quantum computers, Shor's algorithm [10]. For a quantum computer with a number of entangled qubits of the order $O((\ln n)^2(\ln \ln n)(\ln \ln \ln n))$, the factorisation time becomes of the order $O(b^3)$ [11], much faster than the GNFS.

There are many other examples of problems, both theoretical and practical, that can be solved by quantum computing, from increasing the precision of the diagnosis and distribution of medicines [12], to the prediction of weather patterns [13]. The leaps that can be made in these fields make part of the motivation for the development of quantum computers.

Although the benefits of the development of quantum computers is clear, much like classical computers, there are significant obstacles to overcome. One of these is the issue of *scalability*, which has been discussed in this chapter. Quantum systems, particularly entangled systems, are sensitive to environmental disturbances. Dependant on the system, magnetic field, electric field, temperature and even positional disturbances can cause *decoherence*, the destruction of quantum entanglement.

As the reduction of the time taken in the factorisation of large numbers given by Shor's algorithm is dependant on having a large number of entangled qubits, without the development of extremely reliable qubits, resistant to decoherence, Shor's algorithm (as well as every other use for quantum computing) will not be realised. These qubits, and the subsequent quantum gates, must have a very high *fidelity*; a measure of a qubits resistance to the infidelities that cause decoherence.

There are several methods being explored for their potential to realise high fidelity qubits, such as superconduction [14, 15], or the use of photons in linear optical quantum computing [16]; this thesis focuses on trapped ions, which have long been at the forefront of innovations in the realm of quantum computing [17]. Many of the proposals for the use of trapped ions in quantum computing used different methods of entangling the qubits, but all consisted of ions confined in a linear trap, greatly restricting their positional movement to one axis [18, 19], taking inspiration and building upon the previous models and the Sørensen and Mølmer model [17] which was one of the first papers to suggest this kind of quantum gate.

Various iterations through the years have resulted in the experimental demonstration of very high fidelity gates [20, 21], resulting in the increase of the fidelity threshold for a useful quantum gate from 0.97, which was sufficient for a single gate, to 0.9999 [22], as for large scale, useful quantum computing, very small infidelities in the individual gates

compound quickly. To achieve this high fidelity threshold, the gates must be capable of error correction [23], meaning they can correct errors during their own gate operation, which is analogous to classical computing gates.

The gates must also have a very small gate operation time or a long coherence time [24]. This is one of the clear advantages in the use of Rydberg ions in quantum information processing; they have very strong dipole-dipole interactions, even over long distances, which makes interaction and building entanglement between qubits much faster. In turn, increasing the gate speed will avail less time for the qubits to decohere.

A potential source of infidelity within Rydberg ion gates is the excitation of the vibrational, or phonon modes of the ions. These where purposefully excited in the Sørensen and Mølmer gate and used to entangle the qubits, however they could be now be a hindrance to the operation of the gate. This project is focused on answering this question.

In chapter two I will present a brief history of quantum computing. Starting with the very first theoretical proof of the possibility of quantum computing, using solutions to Schrodinger's equation to show the legitimacy of the idea of creating a computer using quantum systems. Then focusing on the use of trapped atoms/ions in quantum computing, we will then present the major proposals, and there evolution through the years. The chapter will describe the advantages of each iteration, and the short-comings that led to the next version.

Chapter three will consist of the building of the mathematical model that describes the behaviour of trapped Rydberg ions that would be used in a quantum computer, and analysing certain characteristics of that behaviour. Starting will a general solution to Schrodinger's equation for an atom coupled to a laser field, this solution will be simplified into the Jaynes-Cummings model where quantum phenomena like Rabi oscillations can be observed. The dipole-dipole interaction of the Rydberg ions will then be added to the model in lieu of the next chapter.

Then, in chapter four we will use the full model for two trapped Rydberg ions to evaluate the efficacy of their use in quantum gates, specifically a controlled-Z gate. The dynamics of the spin states, phonon states and their effect on the fidelity of the gate will be explored, during the gate operation.

Finally, the conclusion will be given in chapter five, where we will present, given both the advantages and disadvantages shown in earlier chapters, whether Rydberg ions are an efficient enough material for the manufacture of large scale quantum computers.

Chapter 2

Quantum Computing Background

2.1 Introduction of Quantum Computing

2.1.1 First Proposals of Quantum Computing

A paper by Paul Benioff [25], published in April 1980, gave the first abstract description of a quantum computer or Turing machine as it was described. The paper generally describes and proves that for any given Turing machine (the name given to the general computer described by Alan Turing in one of his first papers [26], but can be used as a substitute for any classical computer gate), denoted in the paper by Q, and any number of quantum particles N, there will exist a specific Hamiltonian H_Q^N and initial states $\Psi_Q^N(0)$ that will satisfy the equation

$$\Psi_Q^N(t) = \exp(-iH_Q^N t)\Psi_Q^N(0).$$

This equation would then describe the first, second, third and so on, completed step of the computation of Q.

Being the first real proposal for quantum computation, the discussion is very abstract, focusing on the proof of concept, rather than any practical applications. However, in 1982, Benioff expanded on his work with another paper [27] published that year. This paper was far more practical, focusing on the use of multiple, entangled spin $1/2$ particles in a finite lattice, each completing separate parts of the computation. Several models were derived for different types of gates, however the significant improvement was the time-independent models ability to not dissipate energy during the steps of their operation.

2.1.2 First Proposals of Quantum Computing using Trapped Atoms

One of the first proposals for quantum computing using ultra-cold atoms in a potential trap was the paper published in 1995 by Cirac and Zoller [1]. They described a series of atoms confined in a linear trap. This, along with the previous laser cooling, restricts their movements to very small oscillations in a single direction. Each atom would then be driven with its own individual laser. By careful selection of the laser frequency, they show the vibrational normal modes of the ions can be excited, and this collective motion is used to entangle the ions.
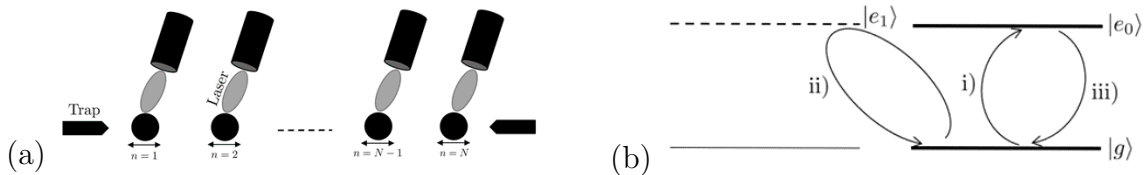
Figure 2.1: A simple diagram and level scheme for the Cirac and Zoller gate [1], shown in (a) and (b) respectively. Figure (a) shows N ions in a linear trap, interacting with N different laser beams. Figure (b) depicts the method in which the CNOT gate is actualised, showing the level scheme for only one of the qubits. The computation basis that makes the qubit is shown in bold ($|g\rangle$ and $|e_0\rangle$), and the other levels do not affect the computation, but are needed to realise the gate.

When in the Lamb-Dicke (LD) limit, and using sufficiently low laser intensities, the centre-of-mass (CM) mode can be excited in the atom, when the laser detuning is equal to the negative of the frequency of the CM mode. Using this, they show the state $|g, 0\rangle_n$ is unaffected, whereas the states $|g, 1\rangle_n$ and $|e, 0\rangle_n$, are transformed as

$$|g, 1\rangle_n \rightarrow \cos(k\pi/2)\,|g, 1\rangle_n - ie^{i\phi}\sin(k\pi/2)\,|e, 0\rangle_n \,,$$
$$|e, 0\rangle_n \rightarrow \cos(k\pi/2)\,|e, 0\rangle_n - ie^{i\phi}\sin(k\pi/2)\,|g, 1\rangle_n \,,$$

where $|g\rangle_n$ and $|e\rangle_n$ represent the ground and excited states of the nth ion respectively and $|0\rangle$ and $|1\rangle$ are the CM mode with zero and one phonon respectively. The wave vector of the applied laser is k and ϕ is a phase added by the process. This is the case only if the laser is applied for the specific amount of time $t = k\pi/(\Omega\eta/\sqrt{N})$ (i.e., using a $k\pi$ pulse), where Ω is the Rabi frequency, η is the LD parameter and N is the total number of atoms. Using this, Cirac and Zoller detailed a process consisting of three steps (denoted as 'i)', 'ii)' and 'iii)' in Fig. 2.1), that would actualise a controlled-NOT (CNOT) gate.

The transformations described above can be summarised by a unitary evolution operator that acts on the system, given by

$$\hat{U}_n^{k,q}(\phi) = \exp[-ik\frac{\pi}{2}(|e_q\rangle_n \langle g|\, \hat{a}e^{-i\phi} + \text{h.c.})],$$

where q is the number of CM mode phonons of the nth ion, $\hat{a}$ is the CM phonon annihilation operator and everything else is as previously defined. Step 'i)' in Fig. 2.1 refers to a π laser pulse of polarisation $q = 0$ and phase $\phi = 0$ on the mth ion. Step 'ii)' shows a 2π laser pulse of of polarisation $q = 1$ and phase $\phi = 0$ on the nth ion. When considering the evolution operator for this system, this second pulse, by rotating through the auxiliary state $|e_1\rangle$, will change the sign of the $|g, 1\rangle$ state. This is also shown by the transformation equations. The final step 'iii)' is the same as the first.

Combining these three steps as one total transformation, and defining $|\pm\rangle = (|g\rangle \pm |e_0\rangle)/\sqrt{2}$, the entire process of the Cirac and Zoller gate can be summarised as $|g\rangle_m |\pm\rangle_n \rightarrow |g\rangle_m |\pm\rangle_n$ and $|e_0\rangle_m |\pm\rangle_n \rightarrow |e_0\rangle_m |\mp\rangle_n$, and this is equivalent to a CNOT gate. More

11

information is given on controlled gates in section 4.1

2.2   Quantum Computing using a Geometric Phase Gate

The gate proposed by Cirac and Zoller was found to be overly sensitive to disturbances, and also had a very long gate operation time, of the order of $10ms$, which proved far too long to width stand quantum decoherence [28, 29], which typically happens on a time scale orders of magnitude less. As a result, through the nineties there were many developments within the field, and by the early 2000s, a common idea for a robust quantum computer was the geometric phase gate.

In 2003, D. Leibfried co-authored a paper [30] that proposed a gate of this kind using two qubit-ions. The main proposal was to construct a gate wherein the qubits where in entangled through phase shifts in position-momentum phase space, making the gate motional sates of the qubit irrelevant to the operation of the gate.

Using the displacement operator,

$$\mathcal{D}(\alpha) = \exp(\alpha a^{\dagger} - \alpha^{\star} a),$$

where $a^{\dagger}$ and a are the creation and annihilation operators respectively, and $\alpha = 1/(2z_0)[\Delta z + i\Delta p/(m\omega)$, where m is the mass of the qubit, ω is the frequency of its harmonic oscillations within the trap, $z_0 = \sqrt{\hbar/(2m\omega)}$ is the spread of the oscillator's ground state wavefunction, and most importantly, Δz and Δp are the displacements in position and momentum space, respectively, the trap potential restricting positional movement to one degree of freedom.

The laser would 'push' the ions along a complete circular path in phase space, returning them to their initial state, with an added phase equal to $\phi = A/\hbar$, where A is the area of the circle who's circumference was traversed in phase space. This idea was generated from the principle that two sequential displacements will produce a phase factor of the form

$$\mathcal{D}(\alpha)\mathcal{D}(\beta) = \mathcal{D}(\alpha + \beta)\exp(i\mathbf{Im}(\alpha\beta^{*})).$$

This additional phase, denoted by $\mathbf{Im}(\alpha\beta^{\star})$, would entangle the qubits, allowing for quantum computation.

This paper claimed an experimentally obtained fidelity of 0.97 with two Be^{+} ions. This fidelity value is usually taken as the minimum requirement for scalable quantum computer (when considering fidelity alone), however the gate's main improvement was in its gate speed, which claimed could be quicker for any given fidelity goal.

This was an effort to circumvent the issues mode gates were having at the time, mainly

susceptibility to magnetic field fluctuations, however this geometric phase gate had its own issues. It was 2.2% likely to spontaneously emit from from states during the gate operation, resulting in decoherence. Also, since the laser was used to drive the qubit along this circular path in phase space, the gate was also sensitive to fluctuations in its detuning.

2.3 Quantum Computing using Trapped Rydberg Particles

2.3.1 Rydberg Atoms and Ions
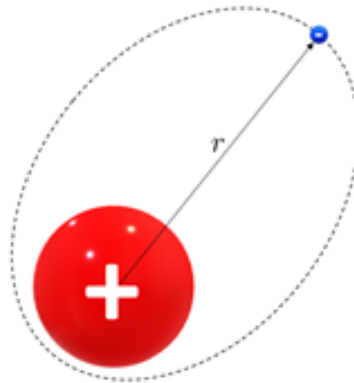
Figure 2.2: A simplified diagram of a Rydberg atom with one electron excited to a Rydberg state. The valence electron is shown in blue, the remainder of the atom shown in red with the distance between the electron and centre of the nucleus shown as $r = 4\pi\epsilon_0 n^2 \hbar^2 / e^2 m$, where n is the principle quantum number of the electron, m is the mass and e the charge of the electron. The groundstate electrons shield the electron in the excited state from the electric field of the nucleus, effectively reducing it to a single positive charge from the reference point of the valence electron, as shown in the figure. The orbitals of electrons excited to Rydberg states can be approximated as semi-classical Bohr orbits under specific conditions [2], hence the depiction in the figure. Figure not to scale.

Rydberg atoms are specific type of excited atom, typically an alkali metal or alkali earth metal (as the valence electrons of these elements have much lower ionisation energies), where one or more electron has been excited to a very high principal quantum number. These Rydberg atoms are then defined as Rydberg *ions* when the overall charge of the particle is not equal to zero.

Usually only one electron is excited to this high principle quantum number in a Rydberg particle; this results in the valence electron having a relatively large orbit in comparison to the rest of the electrons in the particle, as shown in Fig. 2.2. As a result, the remaining electrons in their respective ground states shield the nucleus charge from the valence electron, thus the electric field potential experienced by the valence electron can be approximated to that experienced by an electron in a hydrogen atom.

Another result of the excitation of the valence electron to a very high principle quantum

number is the strong electric dipole moment characteristic of Rydberg particles. As shown in Fig. 2.2, the valence electron in its Rydberg state has a charge of negative one and the nucleus shielded by the remaining electrons will have an effective charge of plus one (for a Rydberg atom). The orbital distance of the valence electron is also very large, being defined as $r = 4\pi\epsilon_0 n^2 \hbar^2 / e^2 m$, where n is the principle quantum number of the electron, m is the mass and e the charge of the electron. For example, a regular Lithium ion has radius of approximately 128pm, whereas Rydberg Lithium atom where the valence electron has $n = 127$ would have a radius of approximately 1μm. These two properties (namely the charge of the electron and effective charge of the nucleus, and the orbital distance of the valence electron) result in Rydberg particles having very strong electric dipole moments.

There are other phenomena of Rydberg particles, such as the strong Coulomb interaction between Rydberg particles, the longevity of Rydberg states and Rydberg blockades. These, and their uses in quantum computing, will be explained further in the following sections.

2.3.2 Quantum Computing using Rydberg Atom Blockades

An important phenomena present in Rydberg atoms that is used in their implementation in quantum gates is the Rydberg blockade effect [31]. Driving the population of the Rydberg level of a particular atom using a resonant laser has the effect of making the Rydberg transition of the second qubit highly off-resonant, when within a certain distance, typically of the order $10ms$ [32].

CNOT gates are most commonly associated with Rydberg atom gates, and this gate was first demonstrated using Rydberg atoms by Isenhower in 2010 [33].

The procedure is very similar to that of the Cirac and Zoller gate, where we define one qubit as the *control* qubit, and the other as the *target* qubit. By populating the Rydberg state of the first control qubit, pulses can be applied to the target qubit, without out it populating its Rydberg state due to the Rydberg blockade effect. This generates phases on the qubit, specific to the length of the pulse applied, as explained in section 2.1.2. The correct combination of pulses can form a CNOT gate.

However, a problem with this kind of gate is mainly twofold; spontaneous emission from the Rydberg state by the control qubit; then population of the Rydberg state by the target qubit. The probability of each of these events occurring being $P = \pi\Omega^2 / 2V^2$, where Ω is the Rabi frequency and V the Coulomb interaction between the Rydberg states [34].

2.3.3 Quantum Computing using Populated Rydberg States

Entangling the qubit via the Coulomb interaction between the Rydberg states was also proposed in 2000 by D. Jaksch [31], soon after the Sørensen and Mølmer gate. This model, as suggested by the title of the article, was focused on improving the gate speed by using the strong interaction between the Rydberg states to build the entanglement between the qubits.

These were found to improve the gate speed, however the resultant gates were extremely sensitive to the separation of the atoms [35, 36], such that within the dipole-dipole interaction limit (the range of distances where the dipole-dipole interaction is dominant) there were no significant ranges for the value of the atom separation R with high gate fidelities. Within the van der Waals limit (where the atom separation is greater than 8m), these regions could be found when $R \gtrsim 100\mu m$ and the principle quantum number of the Rydberg state was $\gtrsim 200$ [37].

2.3.4   Quantum Computing using Trapped Rydberg Ions

The use of Rydberg ions stemmed from the Rydberg atom gate proposals that used the dipole-dipole interaction between the qubits to build entanglement, with the main goal of increasing the gate speed, thereby decreasing quantum decoherence. These gates have been actualised with some success in decreasing gate speed to the order of $10\mu s$ [38, 18], down to sub-microsecond gate speeds [20]. The mechanism of how these gates work will be explained in the subsequent chapters. The main challenges with Rydberg ion gates are spontaneous emission from the Rydberg state and phonons; vibrational excitations in the ions, and their effect will be the focus of chapter 4. The following chapter will focus on building the Jaynes-Cummings model to explore its dynamics, in lieu of forming a controlled-Z gate with trapped Rydberg ions.

Chapter 3

Dynamics of the Jaynes-Cummings Model

3.1 Building the Jaynes-Cummings Model

3.1.1 Single Qubit Model

To build a model of a controlled-Z gate, we first start with a simple model of a single qubit. The total Hamiltonian describing an atom in the electric field of a plane wave is

$$\hat{H} = \hat{H}_{\text{field}} + \hat{H}_{\text{atom}} + \hat{H}_{\text{int}}. \tag{3.1}$$

The field Hamiltonian takes the form

$$\hat{H}_{\text{field}} = \omega \hat{a}^\dagger \hat{a}, \tag{3.2}$$

where $\hat{a}^\dagger$ and $\hat{a}$ are the phonon creation and annihilation operators of the centre-of-mass (COM) mode [39] respectively and ω is the frequency of the trapping potential.

The atom Hamiltonian takes the form

$$\hat{H}_{\text{atom}} = \omega_L \hat{\sigma}_z, \tag{3.3}$$

where in this case, ω_L is the frequency of the laser, making the detuning of the plane wave laser from the resonant frequency of the system $\Delta = \omega - \omega_L$. The atomic inversion operator is given by $\hat{\sigma}_z = |e\rangle \langle e| - |g\rangle \langle g|$.

The interaction Hamiltonian [40] is given by

$$\hat{H}_{\text{int}} = -\hat{\mathbf{d}} \cdot \hat{\mathbf{E}}. \tag{3.4}$$

Here, $\mathbf{E}$ is the electric field operator of the laser, where the position of the ion is taken as zero and only a single mode of the field is considered, namely the resonant mode. This gives the form

$$\hat{\mathbf{E}} = i\sqrt{\frac{2\pi\omega_L}{V}}\mathbf{u}_L(\hat{a} - \hat{a}^\dagger),$$

where ω_L is the frequency of the laser, V is the potential difference of the trap, and $\mathbf{u}_L$ is the orthonormal field mode. Defining $\mathbf{E}_0 = i\sqrt{\frac{2\pi\omega_L}{V}}\mathbf{u}_L$, the electric field operator becomes

$$\hat{\mathbf{E}} = \mathbf{E}_0\hat{a} + \mathbf{E}_0^\star\hat{a}^\dagger. \tag{3.5}$$

The electric-dipole moment operator of the ion is given by $\mathbf{d}$. In this case, the ion doesn't have an electric-dipole moment when it is in an energy eigenstate, therefore $\langle g|\,\mathbf{d}\,|g\rangle = \langle e|\,\mathbf{d}\,|e\rangle = 0$. This gives the result

$$\hat{\mathbf{d}} = \hat{\sigma}_+ \langle e|\,\hat{\mathbf{d}}\,|g\rangle + \hat{\sigma}_- \langle g|\,\hat{\mathbf{d}}\,|e\rangle .$$

The spin-ladder operators are defined as $\hat{\sigma}_+ = |e\rangle\langle g|$ and $\hat{\sigma}_- = |g\rangle\langle e|$. Taking $\hat{\mathbf{d}}_{eg} = \langle e|\,\hat{\mathbf{d}}\,|g\rangle$, we can rewrite the electric-dipole operator as

$$\hat{\mathbf{d}} = \hat{\mathbf{d}}_{eg}\,|e\rangle\langle g| + \hat{\mathbf{d}}_{eg}^\star\,|g\rangle\langle e| . \tag{3.6}$$

We now can expand (3.4), using (3.5) and (3.6), giving the result

$$
\begin{aligned}
\hat{H}_{\text{int}} &= -\hat{\mathbf{d}} \cdot \hat{\mathbf{E}}, \\
\hat{H}_{\text{int}} &= -(\hat{\mathbf{d}}_{eg}\,|e\rangle\langle g| + \hat{\mathbf{d}}_{eg}^\star\,|g\rangle\langle e|) \cdot (\mathbf{E}_0\hat{a} + \mathbf{E}_0^\star\hat{a}^\dagger), \\
\hat{H}_{\text{int}} &= -(\hat{\mathbf{d}}_{eg} \cdot \mathbf{E}_0\hat{a} + \hat{\mathbf{d}}_{eg} \cdot \mathbf{E}_0^\star\hat{a}^\dagger)\,|e\rangle\langle g| - (\hat{\mathbf{d}}_{eg}^\star \cdot \mathbf{E}_0\hat{a} + \hat{\mathbf{d}}_{eg}^\star \cdot \mathbf{E}_0^\star\hat{a}^\dagger)\,|g\rangle\langle e| , \\
\hat{H}_{\text{int}} &= -\frac{1}{2}[(\Omega\hat{a} + \tilde{\Omega}\hat{a}^\dagger)\,|e\rangle\langle g| - (\tilde{\Omega}^\star\hat{a} + \Omega^\star\hat{a}^\dagger)\,|g\rangle\langle e|]. \tag{3.7}
\end{aligned}
$$

The Rabi frequency is defined as $\Omega = 2(\hat{\mathbf{d}}_{eg} \cdot \mathbf{E}_0)$, and the counter-rotating frequency $\tilde{\Omega} = 2(\hat{\mathbf{d}}_{eg} \cdot \mathbf{E}_0^\star)$.

To simplify the interaction Hamiltonian some more, it must be transformed from the Schrödinger picture to the interaction picture [41]. This transformation 'shares' the time dependence of the system observables between the state vectors and operators. This allows many approximations to be made, in this case the rotating wave approximation.

First, a unitary transformation must be performed on the Hamiltonian. We can define the Schrödinger picture Hamiltonian as

$$\hat{H} = \hat{H}_{0,\mathbf{s}} + \hat{H}_{1,\mathbf{s}},$$

where $\hat{H}_{0,\mathbf{S}} = \hat{H}_{\text{field}} + \hat{H}_{\text{atom}}$ and $\hat{H}_{1,\mathbf{S}} = \hat{H}_{\text{int}}$. This choice of $\hat{H}_{0,\mathbf{S}}$ is made as these parts of the total Hamiltonian are exact and solvable, with no explicit time dependence. Now the transformation matrix can be defined as

$$\hat{U} = \exp(i\hat{H}_{0,\mathbf{S}}t), \tag{3.8}$$

and the unitary transformation to the interaction picture

$$\hat{H}_{1,\mathbf{IP}} = \hat{U}\hat{H}_{1,\mathbf{S}}\hat{U}^{\dagger},$$
$$\hat{H}_{1,\mathbf{IP}} = -\frac{1}{2}[(\Omega\hat{a}e^{-i(\omega-\omega_L)t} + \tilde{\Omega}\hat{a}^{\dagger}e^{i(\omega+\omega_L)t})\,|e\rangle\,\langle g| + (\tilde{\Omega}^{\star}\hat{a}e^{-i(\omega+\omega_L)t} + \Omega^{\star}\hat{a}^{\dagger}e^{i(\omega-\omega_L)t})\,|g\rangle\,\langle e|], \tag{3.9}$$

defining the ground state to be the zero of energy.

We now assume the relationship between the atomic transition and laser frequency $\omega_L \approx \omega$. With this condition, the exponential terms oscillating at frequency $\omega - \omega_L \approx 0$ are approximately resonant, and the counter-rotating exponential terms oscillating at $\omega + \omega_L \approx 2\omega_L$, approximately anti-resonant. The rotating wave approximation states that under the conditions assumed here, $\Delta \ll (\omega + \omega_L)$, the counter-rotating terms can be neglected [42]. This is because these terms describe the coupling between states with very large energy differences, in comparison to the coupling strength. This results in very little population change between these states being a result of the coupling.

This effect can also be seen by comparing the timescales of the resonant and anti-resonant behaviour. Defining the following periods;

$$\tau_1 = \frac{2\pi}{\Delta}; \tag{3.10}$$

$$\tau_2 = \frac{2\pi}{\omega + \omega_L} \approx \frac{2\pi}{2\omega_L}, \tag{3.11}$$

τ_1 being the resonant period, and τ_2 the anti-resonant. It is clear that $\tau_1 \gg \tau_2$, resulting in the anti-resonant terms completing many full oscillations during one resonant time period. These oscillations will average out to zero over the analysis of these longer timescales, therefore those terms can be ignored.

The resulting interaction Hamiltonian in the interaction picture is

$$\hat{H}_{1,\mathbf{IP}}^{\text{RWA}} = -\frac{1}{2}[(\Omega\hat{a}e^{-i(\omega-\omega_L)t})\,|e\rangle\,\langle g| + (\Omega^{\star}\hat{a}^{\dagger}e^{i(\omega-\omega_L)t})\,|g\rangle\,\langle e|]. \tag{3.12}$$

To return back to the Schrödinger picture, we perform a unitary transformation again.

$$\hat{H}_{\text{int}}^{\text{RWA}} = \hat{U}^\dagger \hat{H}_{1,\text{IP}}^{\text{RWA}} \hat{U} \tag{3.13}$$

$$\hat{H}_{\text{int}}^{\text{RWA}} = \frac{\Omega}{2}(\hat{a}\sigma_+ + \hat{a}^\dagger \sigma_-), \tag{3.14}$$

Where for the sake of simplicity, Ω is assumed a real number, and it has absorbed the negative sign. We can now write the full Hamiltonian as,

$$\hat{H} = \hat{H}_{\text{field}} + \hat{H}_{\text{atom}} + \hat{H}_{\text{int}}^{\text{RWA}},$$

$$\hat{H} = \omega \hat{a}^\dagger \hat{a} + \omega_L \hat{\sigma}_z + \frac{\Omega}{2}(\hat{a}\sigma_+ + \hat{a}^\dagger \sigma_-). \tag{3.15}$$

The dynamics of this Hamiltonian can be analysed by considering the Rabi oscillations of the system. If initial state of the system is prepared as $|\Psi(0)\rangle = |e, 0\rangle$, the evolution through time of that state will be

$$|\Psi(t)\rangle = \cos(\frac{\Omega t}{2}) |e, 0\rangle - i\sin(\frac{\Omega t}{2}) |g, 1\rangle \,.$$

It then follows the probability of of the states $|e, 0\rangle$ and $|g, 1\rangle$ will be

$$\mathcal{P}_{e,0} = \cos^2(\frac{\Omega t}{2}), \tag{3.16}$$

$$\mathcal{P}_{g,1} = \sin^2(\frac{\Omega t}{2}). \tag{3.17}$$

This phenomena is due to the coupling between the atom and the field and can be modelled using only this part of the Hamiltonian. This coupling forms new eigenstates in the system, known as *dressed* states, which are a supersition of the states $|e, 0\rangle$ and $|g, 1\rangle$.

In the perfectly resonant case, the dressed states will be given by [43]

$$|1, \pm\rangle = \frac{1}{\sqrt{2}}(|g, 1\rangle \mp |e, 0\rangle).$$

The Rabi oscillations of the Jaynes-Cummings model in (3.14) are shown in Fig. 3.1, where all parameters are set to 1 for simplicity and the atom and field Hamiltonians are not specifically needed for the Rabi oscillations to be seen.
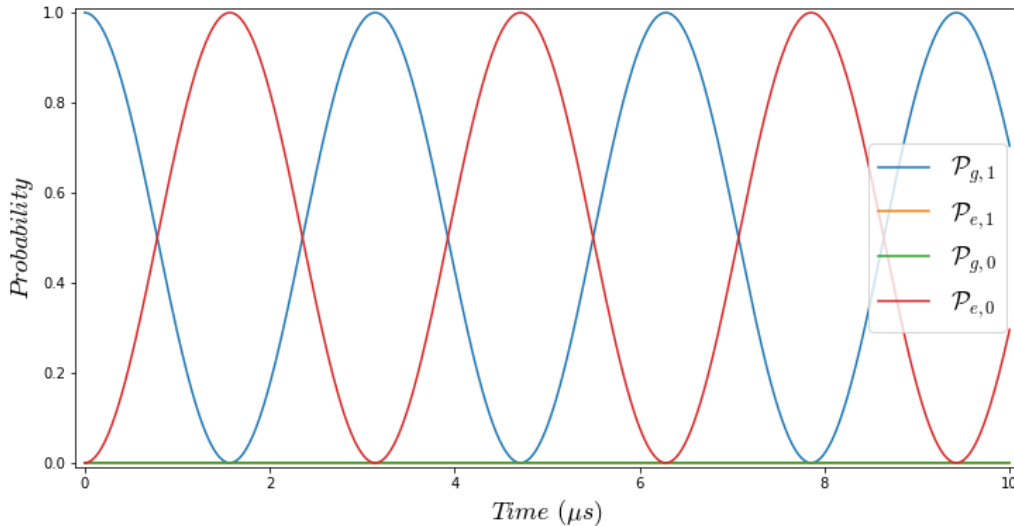
Figure 3.1: The dynamics of the Jaynes-Cummings model shown in (3.14) is shown in this figure. The initial state is set to be $|g, 1\rangle$ and the parameter Ω is set to unity. The only two states excited are the initial state and $|e, 0\rangle$. The model is limited to two allowed phonon modes; the ground state $|0\rangle$ and the excited state $|1\rangle$.

3.1.2 Simple Double Qubit Model

We can extend the system described in the previous section by adding a second atom, making the interaction Hamiltonian that models the Rabi oscillations

$$\hat{H} = \frac{\Omega}{2}(\hat{a}^{(1)}\sigma_+^{(1)} - \hat{a}^{(1)\dagger}\sigma_-^{(1)} + \hat{a}^{(2)}\sigma_+^{(2)} - \hat{a}^{(2)\dagger}\sigma_-^{(2)}), \tag{3.18}$$

where the superscript (n) denotes the nth atom. A method using the probability coefficients of all possible states can be used to solve and display the dynamics of this system.

We start with the time-dependant Schrödinger equation

$$i\hbar\frac{\partial}{\partial t}|\Psi(t)\rangle = \hat{H}|\Psi(t)\rangle.$$

Now consider an arbitrary state $|\phi(t)\rangle$, which is a supersition of the form

$$|\phi(t)\rangle = \sum_{m,n=0}^{N} \mathcal{C}_{gg,mn}(t)|gg,mn\rangle + \mathcal{C}_{ge,mn}(t)|ge,mn\rangle + \mathcal{C}_{eg,mn}(t)|eg,mn\rangle + \mathcal{C}_{ee,mn}(t)|ee,mn\rangle, \tag{3.19}$$

where $\mathcal{C}_{gg,mn}(t)$ is the time-dependant probability coefficient of the state $|gg,mn\rangle$, with the rest following suit, and N is the number of phonon modes.

We can now act on this state with the Hamiltonian, using the following rules for the operators;

$$
\begin{aligned}
\hat{a}\left|n\right\rangle &= \sqrt{n}\left|n-1\right\rangle, \\
\hat{a}^{\dagger}\left|n\right\rangle &= \sqrt{n+1}\left|n+1\right\rangle, \\
\hat{\sigma}_{+}\left|g\right\rangle &= \left|e\right\rangle, \\
\hat{\sigma}_{-}\left|e\right\rangle &= \left|g\right\rangle,
\end{aligned}
$$

to give the result

$$
\begin{aligned}
\hat{H}\left|\phi(t)\right\rangle = \frac{\Omega}{2}[& \mathcal{C}_{ee,01}(t)\left|eg,00\right\rangle + \mathcal{C}_{ee,10}(t)\left|ge,00\right\rangle + \mathcal{C}_{ee,00}(t)\left|eg,01\right\rangle + \mathcal{C}_{ee,00}(t)\left|ge,10\right\rangle \\
& - \mathcal{C}_{ge,11}(t)\left|ee,01\right\rangle + \mathcal{C}_{ge,10}(t)\left|gg,11\right\rangle - \mathcal{C}_{ge,10}(t)\left|ee,00\right\rangle + \mathcal{C}_{ge,00}(t)\left|gg,01\right\rangle \\
& + \mathcal{C}_{eg,11}(t)\left|ee,10\right\rangle - \mathcal{C}_{eg,01}(t)\left|ee,00\right\rangle + \mathcal{C}_{eg,01}(t)\left|gg,11\right\rangle + \mathcal{C}_{eg,00}(t)\left|gg,10\right\rangle \\
& + \mathcal{C}_{gg,11}(t)\left|ge,10\right\rangle + \mathcal{C}_{gg,11}(t)\left|eg,01\right\rangle - \mathcal{C}_{gg,01}(t)\left|ge,00\right\rangle - \mathcal{C}_{gg,10}(t)\left|eg,00\right\rangle].
\end{aligned}
\tag{3.20}
$$

Then acting with operators on the left hand side of the Schrödinger equation, we can collect the like terms of the state vectors to give the following series of coupled differential equations;

$$\dot{\mathcal{C}}_{eg,00}(t) = \frac{\Omega}{2}[-\mathcal{C}_{gg,10}(t)]; \tag{3.21}$$

$$\dot{\mathcal{C}}_{ge,00}(t) = \frac{\Omega}{2}[-\mathcal{C}_{gg,01}(t)]; \tag{3.22}$$

$$\dot{\mathcal{C}}_{eg,01}(t) = \frac{\Omega}{2}[\mathcal{C}_{ee,00}(t) - \mathcal{C}_{gg,11}(t)]; \tag{3.23}$$

$$\dot{\mathcal{C}}_{ge,10}(t) = \frac{\Omega}{2}[\mathcal{C}_{ee,00}(t) - \mathcal{C}_{gg,11}(t)]; \tag{3.24}$$

$$\dot{\mathcal{C}}_{gg,10}(t) = \frac{\Omega}{2}[-\mathcal{C}_{eg,00}(t)]; \tag{3.25}$$

$$\dot{\mathcal{C}}_{gg,11}(t) = \frac{\Omega}{2}[\mathcal{C}_{eg,01}(t) + \mathcal{C}_{ge,10}(t)]; \tag{3.26}$$

$$\dot{\mathcal{C}}_{ee,00}(t) = \frac{\Omega}{2}[-\mathcal{C}_{eg,01}(t) - \mathcal{C}_{ge,10}(t)]; \tag{3.27}$$

$$\dot{\mathcal{C}}_{ee,10}(t) = \frac{\Omega}{2}[-\mathcal{C}_{eg,11}(t)]; \tag{3.28}$$

$$\dot{\mathcal{C}}_{gg,01}(t) = \frac{\Omega}{2}[\mathcal{C}_{ge,00}(t)]; \tag{3.29}$$

$$\dot{\mathcal{C}}_{ee,01}(t) = \frac{\Omega}{2}[-\mathcal{C}_{ge,11}(t)]; \tag{3.30}$$

$$\dot{\mathcal{C}}_{eg,11}(t) = \frac{\Omega}{2}[\mathcal{C}_{ee,10}(t)]; \tag{3.31}$$

$$\dot{\mathcal{C}}_{ge,11}(t) = \frac{\Omega}{2}[\mathcal{C}_{ee,01}(t)]. \tag{3.32}$$

Two of these solutions, each with different initial states, are shown in Fig. 3.2(a) and Fig. 3.2(b). The first starts with the $|eg, 01\rangle$ state fully populated. We see very similar oscillations to the those in Fig. 3.1, where the state $|ge, 10\rangle$ is excited, showing the same interplay between the states $|g, 1\rangle$ and $|e, 0\rangle$, but this time with two qubits.

A difference we see however is the states $|ee, 00\rangle$ and $|gg, 11\rangle$ being excited. This results in the behaviour of the $|g, 1\rangle$ and $|e, 0\rangle$ states not being exactly sinusoidal, but rather there is a delay in repopulating the states from zero. This also indicates the process of excitation and de-excitation the system goes through, conserving energy all the while; starting in $|eg, 01\rangle$, energy used to excite the second qubit's phonon is transferred to excite its spin state, giving $|ee, 00\rangle$; at the same time the opposite process is occurring in the first qubit, where the energy used to excite its spin state is transferred to excite its phonon, giving the state $|gg, 11\rangle$. The behaviour of these two intermediate states is sinusoidal. Following, the state $|ee, 00\rangle$ excites the phonon of its first qubit using the energy from its spin state, and the state $|gg, 11\rangle$ excites the spin of its second qubit using the energy from its phonon, both populating the state $|ge, 10\rangle$.

(a)   (b)
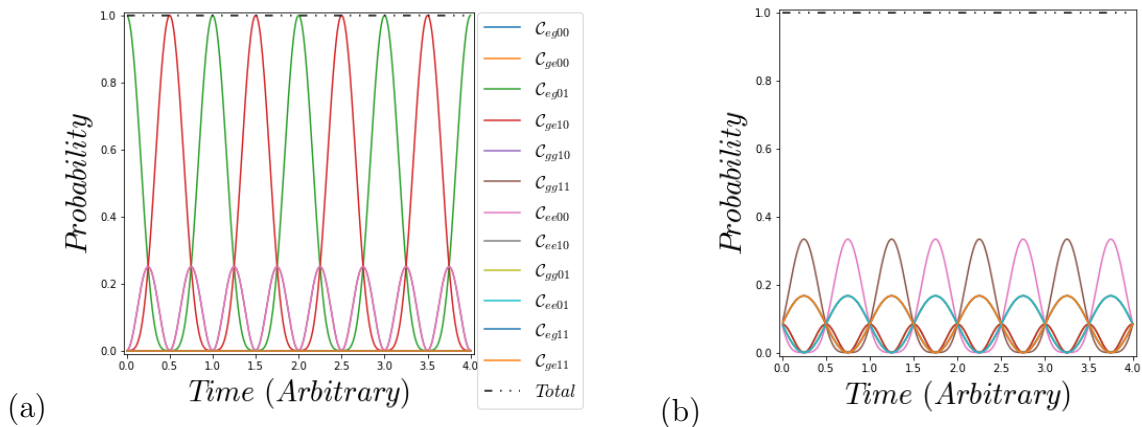
Figure 3.2: The dynamics of the same double spin Jaynes-Cummings model, but with two different initial states, with the Hamiltonian of the system is given in (3.18). The dynamics of the Hamiltonian (3.18) where the initial state is prepared as $\mathcal{C}_{eg01} = 1$ is shown in Figure (a). As a result, the states $\mathcal{C}_{ge10}$, $\mathcal{C}_{gg11}$ and $\mathcal{C}_{ee00}$ are also excited, as they are coupled to the initial state. Figure (b) shows the dynamics when the initial state is a supersition of equal probability between all the states $(1/\sqrt{12})$. The states $\mathcal{C}_{gg11}$ and $\mathcal{C}_{ee00}$ both peak at approx. 0.33, 180 degrees out of phase. The states $\mathcal{C}_{gg10}$, $\mathcal{C}_{gg01}$, $\mathcal{C}_{ge11}$, $\mathcal{C}_{eg11}$, and the states $\mathcal{C}_{ge00}$, $\mathcal{C}_{eg00}$, $\mathcal{C}_{ee10}$ and $\mathcal{C}_{ee01}$ all peak at 0.167; the two groups of states being 180 degrees out of phase again. Lastly, the state $\mathcal{C}_{ge10}$ peaks at approx. 0.083, with twice the period of the other states, as it is uncoupled.

3.1.3   Full Double Qubit Model

MW-Dressing of Ions

Similar to the methods used in Rydberg atom gates described in section 2.3.3, Rydberg *ion* gates aim to populate the Rydberg states and use their strong dipole-dipole interactions to build the entanglement between the qubits [38, 20]. The process requires pumping of the ions to the Rydberg state by separate lasers, then dressing with a microwave field. This results oscillating dipole moments in the ions, giving rise to the dipole-dipole interactions.

To model this effect, the remainder of this project will use a time dependant Rabi frequency and detuning of the form

$$\Omega(t) = \Omega_0 \sin^2(\frac{\pi t}{t_f}), \tag{3.33}$$

$$\Delta(t) = \Delta_0 \cos^2(\frac{\pi t}{t_f}). \tag{3.34}$$

where the parameters $\Omega_0 = 0.1$, $\Delta_0 = 1.7$ and the final time $t_f = 114.85/\Omega_0$ are used. Both the Rabi frequency and the detuning are shown together in Fig. 3.3.
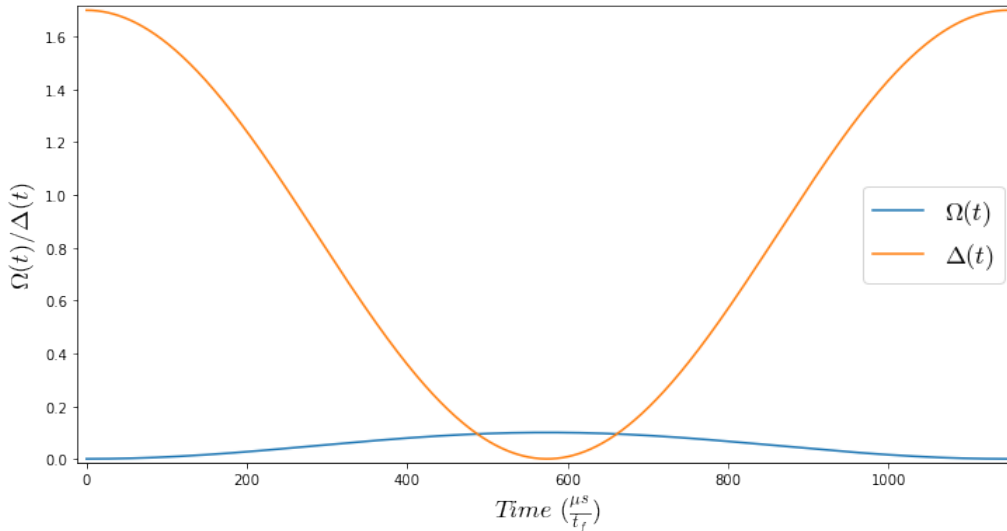
Figure 3.3: The Rabi frequency in (3.34) and the detuning in (3.34) are shown in blue and orange, respectively. The parameters used are $\Omega_0 = 0.1$, $\Delta_0 = 1.7$ and the final time $t_f = 114.85/\Omega_0$.

Derivation of Field Interaction Hamiltonian

Deriving the double spin model of the laser-ion coupling requires a different method to that of the single spin as many-body physics techniques are needed. We start with a general Lagrangian describing the displacement of ions from their equilibrium positions, when coupled by their Coulomb interactions [39],

$$L = \frac{M}{2} \sum_{m=1}^{N} (\dot{q_m})^2 - \frac{1}{2} \sum_{n,m=1}^{N} q_n q_m [\frac{\partial^2 V}{\partial x_m \partial x_n}]_0. \tag{3.35}$$

What is of importance here is the final sum, where q_m is the small deviation in the position of the mth ion, given by x_m. The zero after the partial derivatives denotes they are being evaluated at $q_m = q_n = 0$. These partial derivatives can be solved directly, giving a matrix

$$L = \frac{M}{2} [\sum_{m=1}^{N} (\dot{q_m})^2 - \nu^2 \sum_{n,m=1}^{N} A_{nm} q_n q_m], \tag{3.36}$$

where ν is the trap frequency. The eigenvectors of the matrix A_{nm}, for $N = 2$ are given by

24

$$\mathbf{b}^{(1)} = \frac{1}{\sqrt{2}} \, (1,1), \tag{3.37}$$

$$\mathbf{b}^{(2)} = \frac{1}{\sqrt{2}} \, (-1,1) \tag{3.38}$$

We now define a general Hamiltonian describing the coupling between two ions and an electric field as [44]

$$\hat{H}_{\text{int}} = \frac{\Omega(t)}{2}(\hat{\sigma}_+^{(1)} e^{i\mathbf{k}\cdot\mathbf{x}^{(1)}} + \hat{\sigma}_+^{(2)} e^{i\mathbf{k}\cdot\mathbf{x}^{(2)}} + \text{h.c.}), \tag{3.39}$$

defining the laser wave vector as $\mathbf{k} = 2\pi/\lambda$, where λ is the wavelength of the applied laser, the position of the nth ion as the displacement vector $\mathbf{x}^{(n)}$ and $\Omega(t)$ as the time dependant Rabi frequency, given by (3.34).

The motion of the ions are coupled by their Coulomb interactions, so we define $\mathbf{x}^{(1)}$ and $\mathbf{x}^{(2)}$ as

$$\mathbf{x}^{(1)} = l_1(\hat{a}_1 + \hat{a}_1^\dagger) + l_2(\hat{a}_2 + \hat{a}_2^\dagger), \tag{3.40}$$

$$\mathbf{x}^{(2)} = l_1(\hat{a}_1 + \hat{a}_1^\dagger) - l_2(\hat{a}_2 + \hat{a}_2^\dagger), \tag{3.41}$$

where the minus sign in the equation defining $\mathbf{x}^{(2)}$ comes from the vector mode in (3.38). We also define the oscillator length $l_n = \sqrt{\hbar/2m_n\nu_n}$, where m_n and ν_n are the mass and frequency of the nth ion, respectively.

We now expand the exponential terms in (3.39) up to the first order, giving the equation

$$\hat{H}_{\text{int}} = \frac{\Omega(t)}{2}[\hat{\sigma}_x^{(1)} + \hat{\sigma}_x^{(2)} + \eta_1(\hat{a}^{\dagger(1)} + \hat{a}^{(1)})(\hat{\sigma}_y^{(1)} + \hat{\sigma}_y^{(2)}) + \eta_2(\hat{a}^{\dagger(2)} + \hat{a}^{(2)})(\hat{\sigma}_y^{(1)} - \hat{\sigma}_y^{(2)})], \tag{3.42}$$

where $\sigma_x^{(n)} = (1/2)(\sigma_+^{(n)} + \sigma_-^{(n)})$ and $\sigma_y^{(n)} = (1/2i)(\sigma_+^{(n)} - \sigma_-^{(n)})$ and the Lamb-Dicke parameter $\eta_n = kl_n$.

Equation (3.39) has already had the various approximations described in section 3.1.1 and is essentially a Jaynes-Cummings model [45].

What must also be noted is that the Taylor expansion is only made possible when the conditions of being in the Lamb-Dicke regime are met. If we consider a particle in a laser field, the particle having internal states and motional states, the Lamb-Dicke regime is met when the recoil energy of the particle-photon interaction is much smaller than the energy of the motional states. This effectively means the emission or absorption of a

photon has a negligible effect on the motional state of the particle.

More formally, the Franck-Condon coefficients [45] describe this probability of the absorption or emission of a photon changing the motional state of a particle, and they are given by

$$F_{n\to m} = \langle m| \exp(ik_x x) |n\rangle = \langle m| \exp(i\eta(\hat{a} + \hat{a}^\dagger)) |n\rangle, \tag{3.43}$$

where the probability is for the transition from motional state $|n\rangle$ to $|m\rangle$, with k_x being the projection of the laser wavevector on the x direction and η the Lamb-Dicke parameter. When meeting the conditions for the Lamb-Dicke regime, we can make the following Taylor expansion

$$\exp(i\eta(\hat{a} + \hat{a}^\dagger)) = 1 + i\eta(\hat{a} + \hat{a}^\dagger) + O(\eta^2), \tag{3.44}$$

where the terms $O(\eta^2)$ and above can be ignored.

Dipole-Dipole Interaction between Rydberg Ions

Lastly, a dipole-dipole interaction term must be added to the Hamiltonian to complete the model. This interaction takes the form [46]

$$V_{dd} = \frac{1}{4\pi\epsilon_0} \frac{\mathbf{d}_1 \cdot \mathbf{d}_2 - 3(\mathbf{n} \cdot \mathbf{d}_1)(\mathbf{n} \cdot \mathbf{d}_2)}{R^3}, \tag{3.45}$$

where ϵ_0 is the permittivity of free space, $\mathbf{d}_n$ is the dipole moment of the nth ion, and $\mathbf{n}$ is the normal vector parallel to the direction of the vector connecting the two ions. Expanding this expression, we get the result

$$
\begin{aligned}
\hat{V}_{dd} = \frac{1}{4\pi\epsilon_0 R^3} [& \mathcal{A}_1(\theta)(\hat{d}_{1+}\hat{d}_{2-} + \hat{d}_{1-}\hat{d}_{2+} + 2\hat{d}_{1z}\hat{d}_{2z}) \\
& + \mathcal{A}_2(\theta)(\hat{d}_{1+}\hat{d}_{2z} - \hat{d}_{1-}\hat{d}_{2z} + \hat{d}_{1z}\hat{d}_{2+} - \hat{d}_{1z}\hat{d}_{2-}) \\
& - \mathcal{A}_3(\theta)(\hat{d}_{1+}\hat{d}_{2+} + \hat{d}_{1-}\hat{d}_{2-})].
\end{aligned}
\tag{3.46}
$$

Here the components of the dipole operator in the circular basis are defined as $\hat{d}_{n\pm} = \mp(\hat{d}_{nx} \pm i\hat{d}_{ny})/\sqrt{2}$, where $\hat{d}_{ni}$ is the dipole operator for the nth ion for axis i in the Cartesian basis. We also have the angular prefactors, given by [47],

$$\mathcal{A}_1(\theta) = \frac{(1 - 3 \, \cos^2\theta)}{2},$$

$$\mathcal{A}_2(\theta) = \frac{3 \, \cos \, \theta \, \sin \, \theta}{\sqrt{2}},$$

$$\mathcal{A}_3(\theta) = \frac{3 \, \sin^2\theta}{2},$$

where θ is the angle between the electric field and the normal vector $\mathbf{n}$ described earlier. We know for the experimental setup we are modelling, the linear trap, this angle θ will be approximately zero, resulting in $\mathcal{A}_2 = \mathcal{A}_3 \approx 0$ and $\mathcal{A}_1 \approx -2$. We can therefore simplify (3.46) to

$$\hat{V}_{dd} \approx \frac{-1}{2\pi\epsilon_0 R^3}(\hat{d}_{1+}\hat{d}_{2-} + \hat{d}_{1-}\hat{d}_{2+} + 2\hat{d}_{1z}\hat{d}_{2z}).$$

Now expanding the circular dipole operators into the Cartesian basis, we get

$$\hat{V}_{dd} \approx \frac{-1}{2\pi\epsilon_0 R^3}(\hat{d}_{1x}\hat{d}_{2x} - \hat{d}_{1y}\hat{d}_{2y} + 2\hat{d}_{1z}\hat{d}_{2z}).$$

Again considering the linear trap experimental setup modelled by this Hamiltonian, we know that the dipole moments in the x and y directions will be negligible, making $\hat{d}_{nx} = \hat{d}_{ny} \approx 0$. We can also redefine the dipole operator in the z direction as $\hat{d}_{nz} = d_z\hat{\sigma}_{nz}$, where $\hat{\sigma}_{nz} = |e\rangle \langle e| - |g\rangle \langle g|$ is the Pauli z matrix for the nth ion and d_z is the dipole operator coefficient. Combining this coefficient with the fraction at the beginning of the equation, the dipole-dipole interaction becomes

$$\hat{V}_{dd} \approx V\hat{\sigma}_{1z}\hat{\sigma}_{2z},$$

where $V = -d_z^2/2\pi\epsilon_0 R^3$. Lastly, we know that the dipole-dipole interaction is only present in the Rydberg state $|e\rangle$. Making this change to the expression, the final dipole-dipole interaction Hamiltonian becomes

$$\hat{V}_{dd} \approx V\hat{\sigma}_{1ee}\hat{\sigma}_{2ee} = \hat{H}_{dd}, \tag{3.47}$$

where $\hat{\sigma}_{ee} = |e\rangle \langle e|$. Combining this with the previous terms, the full Hamiltonian modelling a trapped Rydberg ion gate is given by,

$$\hat{H} = \hat{H}_{\text{field}} + \hat{H}_{\text{atom}} + \hat{H}_{\text{int}} + \hat{H}_{\text{dd}},$$

$$\hat{H} = \omega_1 \hat{a}^{\dagger(1)}\hat{a}^{(1)} + \omega_2 \hat{a}^{\dagger(2)}\hat{a}^{(2)} + \frac{\Delta(t)}{2}(\hat{\sigma}_{ee}^{(1)} + \hat{\sigma}_{ee}^{(2)})$$

$$+ \frac{\Omega(t)}{2}[\hat{\sigma}_x^{(1)} + \hat{\sigma}_x^{(2)} + \eta_1(\hat{a}^{\dagger(1)} + \hat{a}^{(1)})(\hat{\sigma}_y^{(1)} + \hat{\sigma}_y^{(2)})$$

$$+ \eta_2(\hat{a}^{\dagger(2)} + \hat{a}^{(2)})(\hat{\sigma}_y^{(1)} - \hat{\sigma}_y^{(2)})] + V\hat{\sigma}_{ee}^{(1)}\hat{\sigma}_{ee}^{(2)}. \tag{3.48}$$

Here the operator σ_z in (3.3) has been changed to σ_{ee} as the detuning only operates in reference to the Rydberg state $|e\rangle$.

The next chapter will fully introduce the concept of controlled gates, and will use the full Hamiltonian in equation (3.48) to actualise a controlled-Z gate. It will also explore the dynamics of the spin and phonon states in the qubits, and will ultimately discuss whether such a gate has a high enough fidelity to be a good candidate for scalable quantum computing.

Chapter 4

Controlled-Z Phase Gate using Trapped Rydberg Ions

4.1 Definition of Controlled-Z Phase Gate
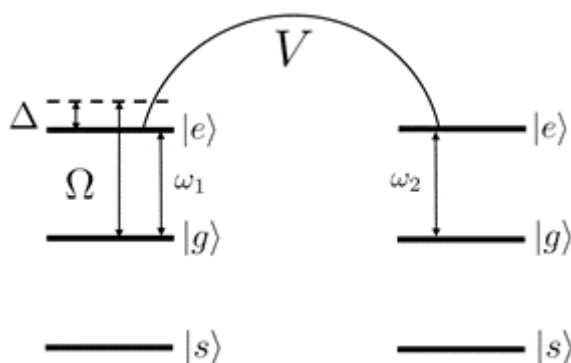
Figure 4.1: The full level scheme for the two qubit system, described by the Hamiltonian in (3.48). The interaction basis is $|gg\rangle, |ge\rangle, |eg\rangle, |ee\rangle$, and the computational basis $|ss\rangle, |sg\rangle, |gs\rangle, |gg\rangle$. The parameters are the laser detuning Δ, the Rabi frequency Ω, ω_1 and ω_2 are the atomic transition frequencies for the first and second ions respectively, and V is the interaction between the $|e\rangle$ states.

A controlled gate is one that operates on at least two qubits, using one as a 'control' qubit, whilst operating on the rest. The control qubit must be in a particular state for the gate to perform the operation on the remaining states [48]. We can define a general, two qubit controlled-U gate as

$$CU = \begin{pmatrix} 1 & 0 & 0 & 0 \\ 0 & 1 & 0 & 0 \\ 0 & 0 & u_{00} & u_{01} \\ 0 & 0 & u_{10} & u_{11} \end{pmatrix}, \tag{4.1}$$

where the operation to be performed on the second qubit if the first is in the state $|1\rangle$ is given by the matrix

$$U = \begin{pmatrix} u_{00} & u_{01} \\ u_{10} & u_{11} \end{pmatrix}. \tag{4.2}$$

29

We get a controlled-Z gate when $U = \sigma_z$, the Pauli z matrix.

Fig. 4.1 shows the full level scheme for the system described by the Hamiltonian in (3.48). We can see two basis in this figure; the *'interaction'* basis $|gg\rangle, |ge\rangle, |eg\rangle, |ee\rangle$ which is used in the Hamiltonian and is the basis coupled to the laser field, and the *'computational'* basis $|ss\rangle, |sg\rangle, |gs\rangle, |gg\rangle$, where the actual computation of the gate will take place, as suggested by its name. As stated earlier, we define a controlled-Z phase gate in this basis by the matrix [49]

$$ CZ = \begin{pmatrix} 1 & 0 & 0 & 0 \\ 0 & 1 & 0 & 0 \\ 0 & 0 & 1 & 0 \\ 0 & 0 & 0 & e^{-i\pi} \end{pmatrix}, \tag{4.3} $$

where the computational basis given before goes with increasing i and j of the elements of the matrix. This means if we have an arbitrary state $|\phi\rangle$ in this basis, given by

$$ |\phi\rangle = \begin{pmatrix} a \\ b \\ c \\ d \end{pmatrix}, $$

and it is acted upon by an ideal CZ gate, the result will be

$$ \hat{CZ}|\phi\rangle = \begin{pmatrix} a \\ b \\ c \\ e^{-i\pi}d \end{pmatrix}. \tag{4.4} $$

Therefore, an ideal CZ gate is one which acts on a state in its computational basis and returns it to its initial state, with a phase of $-\pi$ on the $|gg\rangle$ state [49].

4.2 Populations of Spin and Phonon States during Gate Operation

4.2.1 Spin Populations during Gate Operation

Spin Populations for Ideal States

The Hamiltonian is not in the computational basis, but rather the interaction. This is because its purpose is to describe the mechanism of the interaction and building the entanglement between the two qubits in order for the gate to be realised in the computational basis. Hence the importance of the high-lying Rydberg states $|e\rangle$, as explained in

3.1.3. They have very strong Coulomb interactions, as mentioned in chapter two, which is used to entangle the qubits. The dynamics of the populations of the spin states in the interaction basis can be analysed show a clear picture of this process.

Fig. 4.2 shows the populations of the $|g\rangle$ and $|e\rangle$ states for both qubits, through the gate operation when the Fock state $|gg, 00\rangle$ is used as the initial state. We see that the $|e\rangle$ states of both qubits are populated during the gate operation. This shows the possibility of the entanglement of the qubits.

We also see the states return to their initial sates by the end of the gate operation. For the Fock state used as the initial state, this is expected and further supports an ideal gate operation.
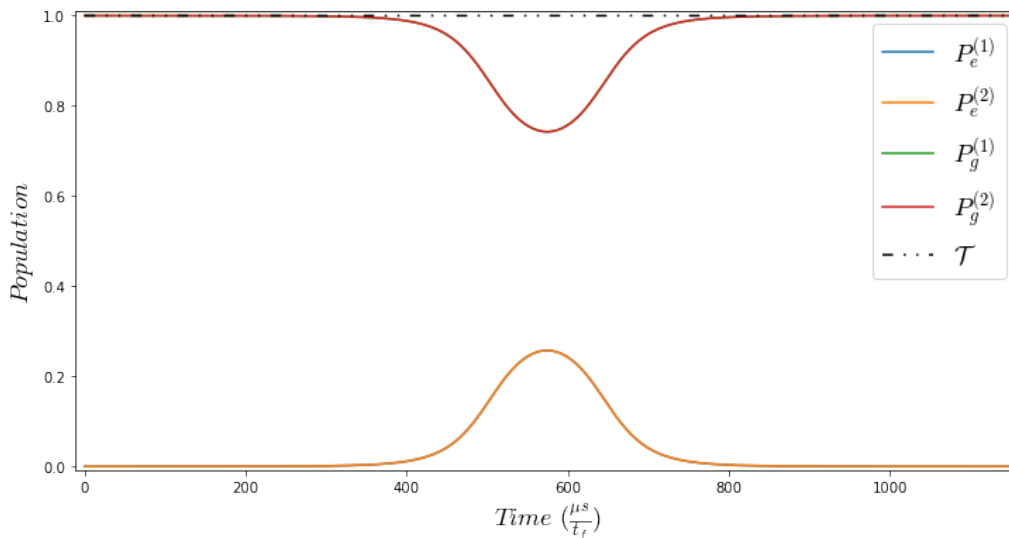
Figure 4.2: The dynamics of the spins during the gate operation, for Fock state $|gg, 00\rangle$, showing a smooth Gaussian form, with the $|e\rangle$ states of both qubits being populated during the gate operation. Notably, the populations of the $|g\rangle$ returns to unity for both qubits. The parameters used are $\Delta_0 = 0.1$, $\Omega_0 = 0.7$, $\omega_1 = 0.1$, $\omega_2 = 0.2$, $l_1 = l_2 = \eta = 0.1$, $V = 1.7$ and the final time $t_f = 118.45/\omega_1$.

Spin Populations for Coherent States

The previous section prepared the initial state in the ideal case of $|gg, 00\rangle$, however this is not realistic as there will always be noise in the system and probability of exciting the phonon modes. Using coherent states will be a better representation of real conditions in a quantum computing gate.

The coherent states are formed using the displacement operator given by

$$\hat{\mathcal{D}}(\alpha) = \exp(\alpha\hat{a}^\dagger - \alpha^\star\hat{a}), \tag{4.5}$$

where for this project, α is a real number. This displacement operator acts as a kind

of 'push' exciting higher phonon modes. A greater α results in a bigger 'push'. For the modelling of a qubit in a quadratic potential, this 'push' results in oscillations [50].

The displacement operator acts as:

$$\hat{\mathcal{D}}(\alpha)\left|0\right\rangle = \left|\alpha\right\rangle.$$

We can model the effect of the displacement operator on the distribution of population of the phonon modes [51] as

$$P_n = \exp(\frac{-|\alpha^2|}{2})\frac{\alpha^n}{\sqrt{n!}}, \tag{4.6}$$

P_n is the population of the nth phonon mode. The distributions for $\alpha = 0.2, 0.5, 2.0$ are shown in Fig. 4.3. In reality, there is an infinite number of phonon modes, each populated to some level, of the form

$$\left|\alpha\right\rangle = e^{-\frac{|\alpha|^2}{2}} \sum_{n=0}^{\infty} \frac{\alpha^n}{\sqrt{n!}} \left|n\right\rangle.$$

However, by knowing the distribution of the populations of the phonon modes, the mathematical model of the Hamiltonian can be truncated to the minimum number of phonon modes needed for an accurate approximation. This decreases the size of the Hilbert space, making the simulations more efficient.
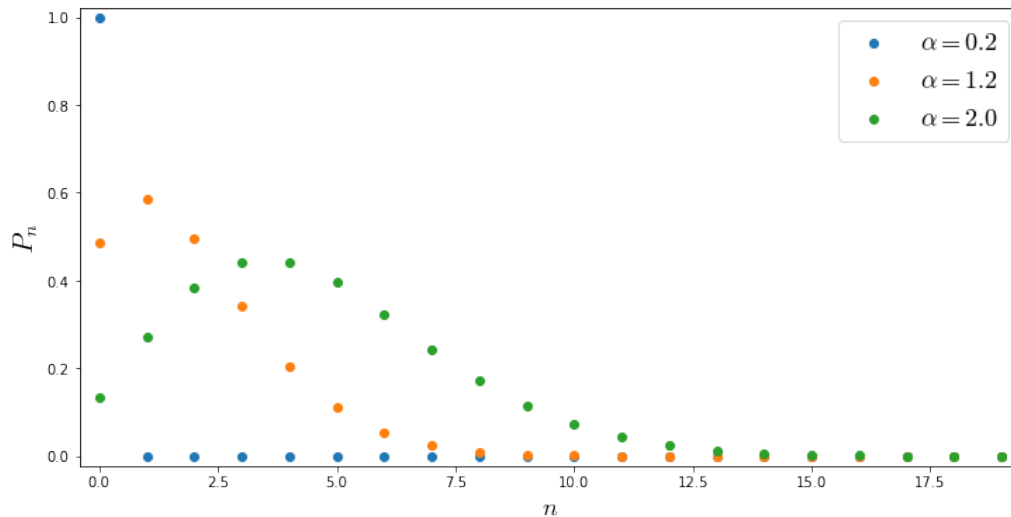
Figure 4.3: The population distribution of the phonon levels for different coherent states. The displacement coefficient α, shown in (4.6), ranges from 0.2 to 2.0. For states with a smaller α, most phonon levels hold a negligible amount of population and can be ignored; for $\alpha = 0.2$, the first two phonon levels hold the majority of the population.

Fig. 4.4 shows the spin population dynamics (calculated by summing the populations of each individual spin state from the complete population matrix) for an initial coherent state $|gg, \alpha\alpha\rangle$, where $\alpha = 0.2, 1.2$. The effect on the dynamics are clear in comparison to the Fock state shown in Fig. 4.2. The general Gaussian form is still present, but there are oscillations in the dynamics which were not present in the Fock state.

What is also important is that the populations of the spin state after the gate operation do not return back to as they were in the initial state; fully populated $|g\rangle$ states. Rather, there is some population remaining in the $|e\rangle$. This relative population at the end of the gate operation increases as α increases. This relationship is shown in Fig. 4.5.

(a)   (b)
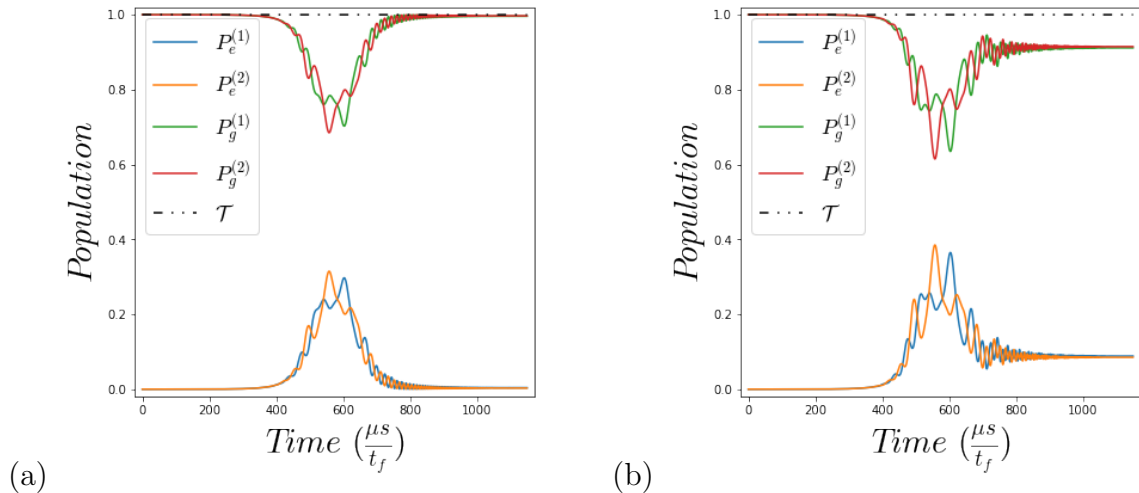
Figure 4.4: The qubit spin dynamics for coherent states with different displacement coefficients α. Figure (a) and Figure (b) shows when $\alpha = 0.2$ and $\alpha = 1.2$ respectively. The initial state is unaffected, however the populations of the spin states during the gate operation and the final state is clearly different from that of the Fock state in Fig. 4.2. The parameters used are $\Delta_0 = 0.1$, $\Omega_0 = 0.7$, $\omega_1 = 0.1$, $\omega_2 = 0.2$, $l_1 = l_2 = \eta = 0.1$, $V = 1.7$ and the final time $t_f = 118.45/\omega_1$ [3].

Fig. 4.5 shows the end population of the $|g\rangle$ state for the first qubit against α, with the model for Fig. 4.5(a) being limited to $N = 2$ and Fig. 4.5(b) limited to $N = 30$. First detail worth noting is the sinusoidal nature of the graphs. This can be explained by the limiting of the phonon modes in the model.

33

(a)

(b)
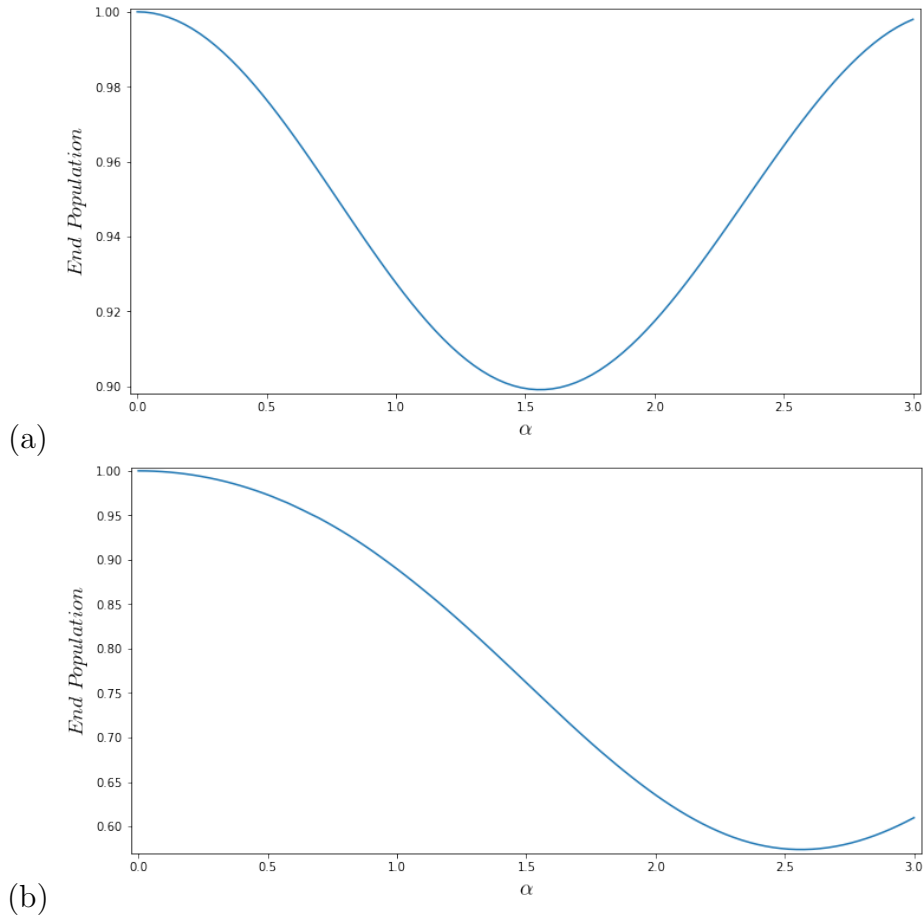
Figure 4.5: The population of the $|g\rangle$ state for the first qubit, at the end of the gate operation. All parameters between the two simulations are the same, with the exception being (a) has $N = 5$ and (b) has $N = 30$. Increasing N increases the amplitude and wavelength of the waveform in the graphs. The parameters used are $\Delta_0 = 0.1$, $\Omega_0 = 0.7$, $\omega_1 = 0.1$, $\omega_2 = 0.2$, $l_1 = l_2 = \eta = 0.1$, $V = 1.7$ and the final time $t_f = 118.45/\omega_1$.

As explained earlier, the displacement operator gives the qubit a 'push', exciting higher phonon modes. In reality, there is an infinite number of phonon modes so increasing α will always result in higher modes being excited, but with a limited model results in a 'rebound', exciting lower phonon modes again.

An analogy would be a force applied to a mass on a rough surface, some distance away from a wall. A small force will result in the mass coming to rest at some displacement before it hits the wall. When increasing the force applied to mass, it will eventually hit the wall and rebound back towards its initial position, decreasing its displacement. This analogy is supported by Fig. 4.5, which shows that when N is increased from 5 to 30, the period and the amplitude of the result in the graph both increase.

4.2.2   Phonon Populations during Gate Operation

Phonon Populations for Ideal States

It is important to see that the dynamics of the spin states during the gate operation doesn't have a sizable effect on the phonon populations for the initial state $|gg, 00\rangle$, although we know there will be very small populations in these states. The dynamics of the phonon modes for the first qubit are shown in Fig. 4.6.

Figure 4.6: The dynamics for the Fock state $|gg, 00\rangle$. This example is somewhat trivial, but nevertheless important to see the change in spin populations doesn't effect the phonon populations.

Phonon Populations for Coherent States

Using the same coherent state model as in (4.2.1), Fig. 4.7 shows the same gate operations as Fig. 4.4, however, the dynamics of the phonon modes for the first qubit are shown instead.

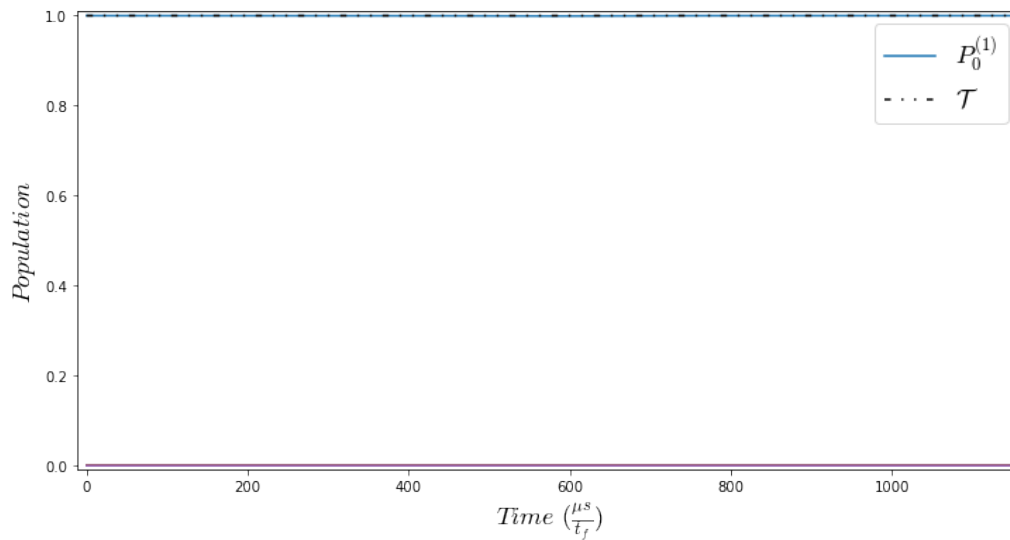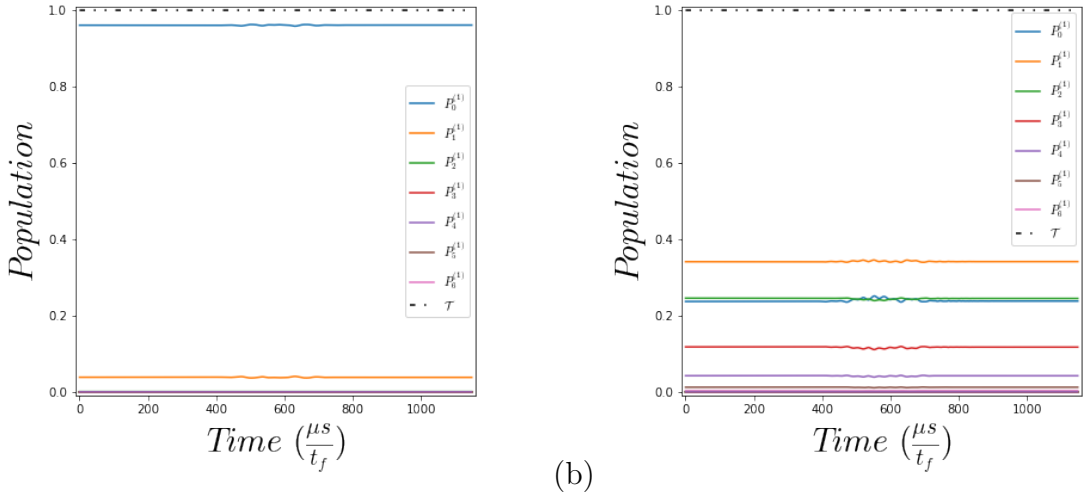Figure 4.7: The phonon dynamics for coherent states with different displacement coefficients, both figures show the first qubit. Figure (a) and (b) show $\alpha = 0.2$ and $\alpha = 1.2$ respectively. The dynamics of the phonon states, during the gate operation, doesn't change significantly with alpha, but rather the relative amount each phonon state is populated. For example, the dynamics of the $|1\rangle$ shown in both figures doesn't change, however for $\alpha = 0.2$, the average population is approximately 0.25 during the gate operation, but for $\alpha = 1.2$, the population is approximately 3.5. The parameters used are $\Delta_0 = 0.1$, $\Omega_0 = 0.7$, $\omega_1 = 0.1$, $\omega_2 = 0.2$, $l_1 = l_2 = \eta = 0.1$, $V = 1.7$ and the final time $t_f = 118.45/\omega_1$.

Unlike the spin dynamics, the phonon dynamics are very stable through the gate operation, the major change with α being the initial populations of each phonon mode, rather than change during the gate operation. This is expected as we know the displacement operator acts to excite higher phonon modes and we see these being excited more so when $\alpha = 1.2$ as opposed to $\alpha = 0.2$. We also know that the interaction basis is formed of the spin states, so more change is expected in these.

Notwithstanding, there are still small deviations in the dynamics of the phonon modes in the same region as the Gaussian peaks/troughs in the spin dynamics. These deviations also become more pronounced when α is increased, meaning when higher phonon modes are excited at the beginning of the gate operation, there is more transfer of population between the phonon states during the gate operation. This would suggest that there is potentially some correlation between the two that is worth exploring further.
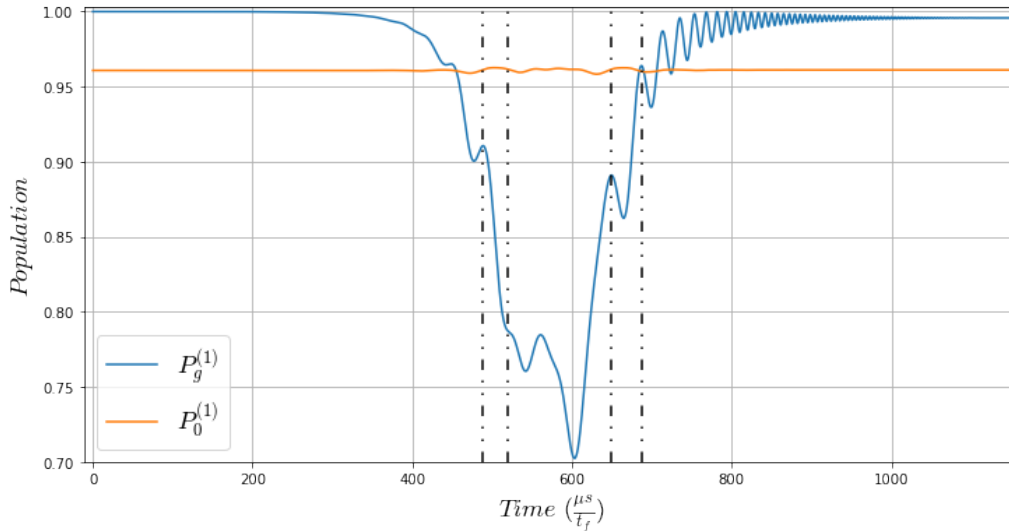
Figure 4.8: The dynamics for a coherent state where the displacement coefficient $\alpha = 0.2$. The populations for the states $|g\rangle$ and $|0\rangle$ are shown. There is overlap between the oscillations in the spin dynamics with the small disturbances in the phonon dynamics, as shown by the vertical dashed lines.

Fig. 4.8 shows this using the dynamics of the $|g\rangle$ and $|0\rangle$ states of the first qubit, when $\alpha = 0.2$. The vertical lines show some correlation between the peaks in the oscillations in the Gaussian of the spin dynamics and the deviations in the phonon dynamics. This could be explained by considering a semi-classical representation of the system; where the ions are flipping 180 degrees between the spin-up and spin-down states, whilst oscillating back and forth within a potential trap. This could be the cause of the deviations in the phonon dynamics. It would also explain the lack of deviations in the phonon dynamics for the Fock state $|gg, 00\rangle$, as in this representation, this ion wouldn't be oscillating within the trap.

There are obviously problems with this representation, for example, the position of an ion within a potential trap will always have a level of uncertainty. However, the representation could help discover the cause of the deviations.

4.2.3   A Simple Definition of the Fidelity of a Quantum Gate

The fidelity of a quantum gate (calculated using the methods described below) can be loosely described as a measure of the gate's quality, and is directly linked with potential for the scalability needed for a true quantum computer [52, 53, 54].

We can define a simple definition of the fidelity as

$$F = \text{Tr}\rho W, \tag{4.7}$$
$$F = \text{Tr}[|\psi_i\rangle \langle\psi_i|t\rangle \langle t|],$$
$$F = \text{Tr}[\langle\psi_i|t\rangle \langle t|\psi_i\rangle],$$
$$F = |\langle\psi_i|t\rangle|^2, \tag{4.8}$$

where ρ is the initial state density matrix, W is the density matrix of the state at time t, $|\psi_i\rangle$ is the initial state and $|t\rangle$ is the state at time t. The resulting fidelity is clearly then the probability of finding the system in its initial state, at any given time.

Fidelity of Gate through Gate Operation
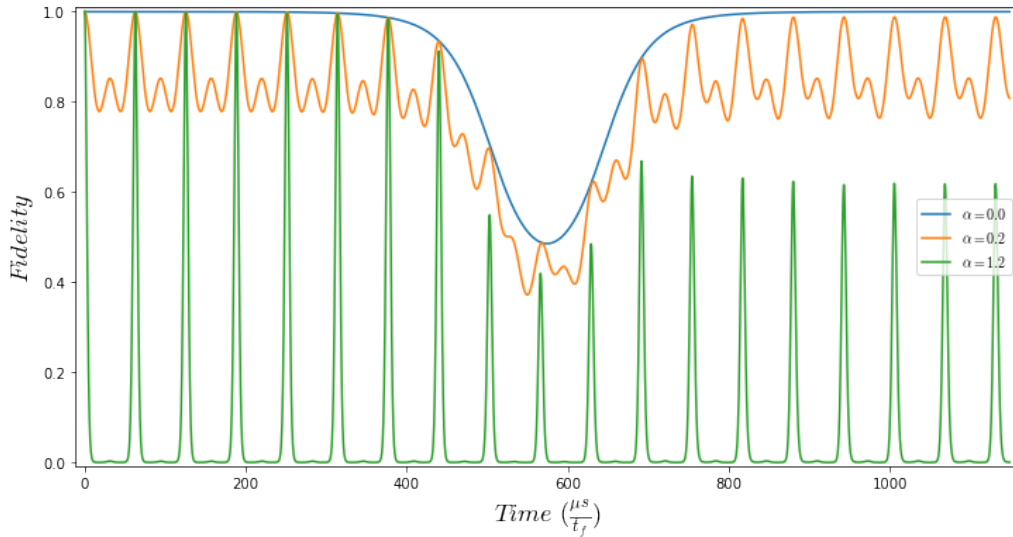
Figure 4.9: The fidelity of the gate through time, calculated using (4.8), for the Fock state $|gg, 00\rangle$ and two different coherent states of the form $|gg, \alpha\alpha\rangle$; $\alpha = 0.2$ and $\alpha = 1.2$ are shown in orange and green respectively. Note how the peaks of the fidelity of the two coherent states never higher than the curve of the Fock state. The parameters used are $\Delta_0 = 0.1$, $\Omega_0 = 0.7$, $\omega_1 = 0.1$, $\omega_2 = 0.2$, $l_1 = l_2 = \eta = 0.1$, $V = 1.7$ and the final time $t_f = 118.45/\omega_1$.

Fig. 4.9 shows the fidelity of the gate through time calculated using (4.8), the initial states being the Fock state $|gg, 00\rangle$ and two coherent states of the form $|gg, \alpha\alpha\rangle$, where $\alpha = 0.2$ and 1.2. The fidelity of the Fock state shows a smooth curve, very similar to that of the spin state dynamics. This is consistent with what is expected, as we know the probability of exciting phonon modes in this case is negligible, therefore the only changes that could effect the fidelity of the gate are the populations of the spin states.

The behaviour changes when the state are displaced initially. Periodic oscillations (the period equal to approx. $6.23/\omega_1$) arise in the fidelity of the gate when using coherent states, with the amplitude of these oscillations increasing as α is increased. At the begin-

ning of the gate operation, the peaks of these oscillations reach the fidelity of the Fock state, but though the gate operation, they fall away a settle to a level lower than the fidelity of the Fock state. The peaks of the coherent state with $\alpha = 1.2$ falls away faster and settles to a lower peak end fidelity than that of the state where $\alpha = 0.2$.

What is also worth noting is that the the period of the oscillations in the fidelity of the coherent states doesn't change at any point during the gate operation, the form of oscillations do, around $t = t_f/2$, and then they settle into a new oscillatory pattern with a different form. This is more clearly seen in the fidelity of the coherent sate where $\alpha = 0.2$.

They falling away of the peaks of the fidelity can be explained by the $|e\rangle$ states of both qubits being slightly populated at the end of the gate operation, as shown in Fig. 4.4(b). However, the oscillations at the beginning of the gate operation cannot be explained by either the spin or phonon dynamics as both are stable when $t < t_f/2$, regardless of α. These oscillations in the fidelity are caused by the *phase* of the various states. This also explains why the oscillations are periodic and why there are none in the Fock state fidelity.

4.3 Robust Definition of the Fidelity of a Controlled 'Z' Phase Gate

4.3.1 Derivation of Robust Definition of Gate Fidelity

With the same general definition of fidelity;

$$F = \mathrm{Tr}\rho W,$$

which is slightly different from (4.8) as we now define $\rho = |\psi_o\rangle \langle\psi_o|$ as the ideal gate output state density matrix. This means $|\psi_o\rangle = \hat{U}_i |\psi_i\rangle$ is the output of an ideal gate $\hat{U}_i$ after operating on an initial state $|\psi_i\rangle$. Then we define $|t\rangle = e^{-i\hat{H}t} |\psi_i\rangle$ as the initial state at a given time t, when being operated on by the actual gate modelled by the Hamiltonian in (3.48). $W = |t\rangle \langle t|$ is the density matrix of the state $|t\rangle$.

The fidelity remains

$$F = |\langle\psi_o|t\rangle|^2, \tag{4.9}$$

however, this can now be expanded in the computational basis, rather than the interaction.

The ideal output state in the computational basis is given by

$$|\psi_o\rangle = \frac{1}{2}[|ss\rangle + e^{-i\phi_g}(|sg\rangle + |gs\rangle) + e^{-i\phi_{gg}} |gg\rangle \otimes \sum_{m,n=0}^{N} \mathcal{C}_{mn}^{(o)} |mn\rangle]. \tag{4.10}$$

The computational basis is as given previously, $|ss\rangle, |sg\rangle, |gs\rangle, |gg\rangle$, the phonon states are denoted in the sum by $|mn\rangle$ and $\mathcal{C}_{mn}^{(o)}$ is the probability coefficient at the end of the ideal gate operation for the phonon state $|mn\rangle$. This will equal zero for all the coefficients, except for the state $|00\rangle$, where $\mathcal{C}_{00}^{(o)} = 1$, by definition of the ideal CZ gate.

The phase factors are found on the $|g\rangle$ states, with ϕ_g denoting the phase on a basis vector with one $|g\rangle$ state, and ϕ_{gg} the phase on the basis vector $|gg\rangle$. Both of these phases are shown in Fig. 4.10(a) and Fig. 4.10(b) respectively.

(a)   (b)
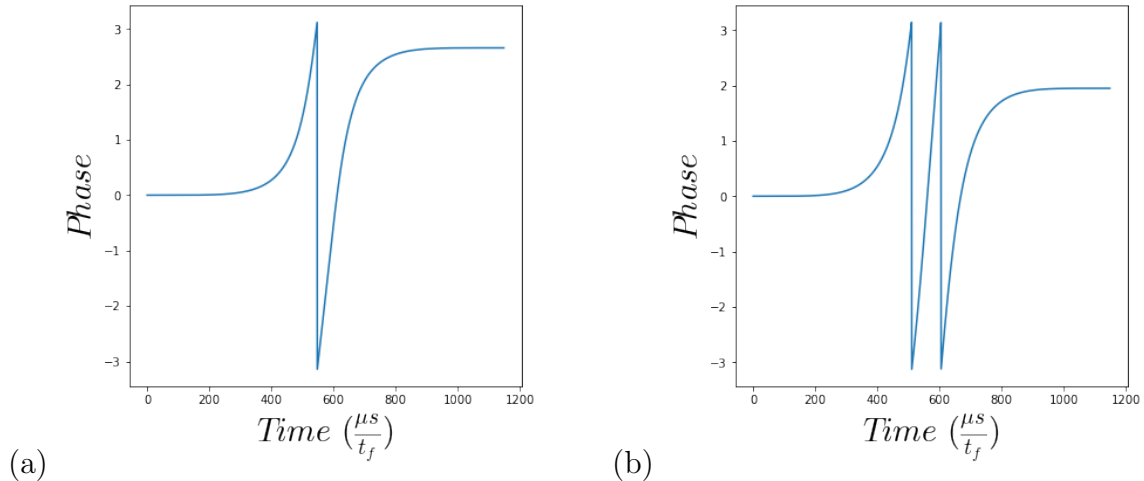
Figure 4.10: The single and double spin phase on the $|gg, 00\rangle$ state during the gate operation, using the full Hamiltonian in (3.48), shown in Figures (a) and (b) respectively. The phase, through the gate operation, of the single spin state $|g, 0\rangle$ is identical to the phase on the state $|gg, 00\rangle$ when there is no interaction between the qubits. The Coulomb interaction $V = 1.7$, the Rabi frequency $\Omega_0 = 0.1$, the laser detuning $\Delta_0 = 1.7$ and the Lamb-Dicke parameter for both qubits $\eta_1 = \eta_2 = 0.1$.

The phase ϕ_g is calculated using a different Hamiltonian than that of ϕ_{gg}. The objective is to find the phase of a single $|g\rangle$ state when operated on by the gate, without any interference from the $|g\rangle$ or $|e\rangle$ state of the other qubit. To achieve this, the Hamiltonian given in (3.48) is changed to remove the parts modelling the interaction and entangled elements between the two qubits, resulting in

$$\hat{H} = \Delta(t)\hat{\sigma}_{ee}^{(1)} + \frac{\Omega(t)}{2}[\hat{\sigma}_x^{(1)} + \eta_1(\hat{\sigma}_y^{\dagger(1)}\hat{a}^{\dagger(1)} + \hat{\sigma}_y^{(1)}\hat{a}^{(1)}) + \eta_2(\hat{\sigma}_y^{\dagger(1)}\hat{a}^{\dagger(2)} + \hat{\sigma}_y^{(1)}\hat{a}^{(2)})]. \quad (4.11)$$

The solution to this Hamiltonian was then used in finding the phase on the single spin state $|g\rangle$.

Entangled Phase

We can rotate the $|g\rangle$ state by ϕ_g, giving the final output state for an ideal CZ gate

$$|\psi_o\rangle = \frac{1}{2}[|ss\rangle + |sg\rangle + |gs\rangle + e^{-i\phi_{ent}}|gg\rangle \otimes \sum_{m,n=0}^{N} \mathcal{C}_{mn}^{(o)}|mn\rangle], \qquad (4.12)$$

where the entangled phase is defined as $\phi_{ent} = \phi_{gg} - 2\phi_g$. This entangled phase, as per the definition a the CZ gate given in (4.3), is $\phi_{ent} = -\pi$ for an ideal gate and initial state. This entangled phase is shown in Fig. 4.11.

The $|gg\rangle$ has the important $e^{-i\pi}$ phase, but importantly this state is coupled with the phonon states $|mn\rangle$. This is because the phonon modes are only present in the interaction basis and the $|g\rangle$ states are also part of that basis.
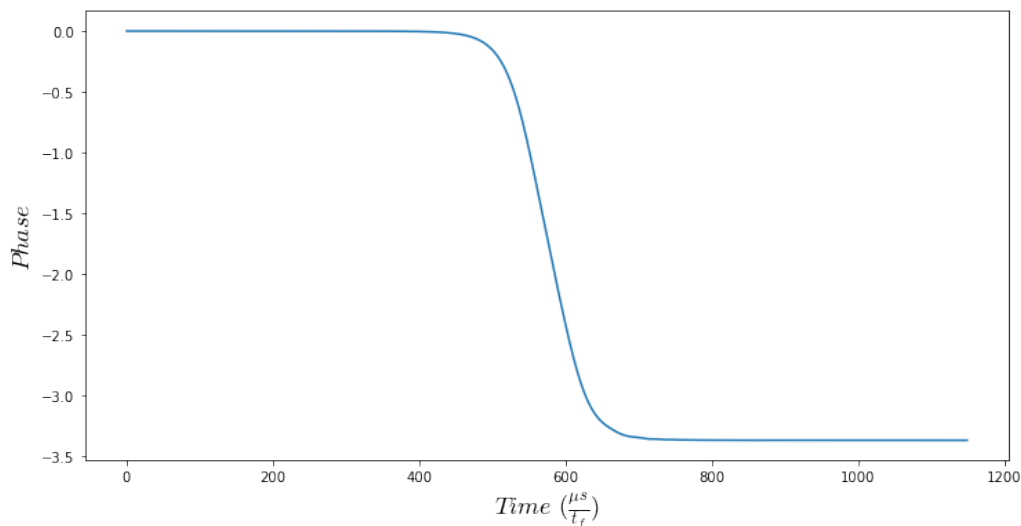
Figure 4.11: The the entangled phase of the state $|gg, 00\rangle$, for the Hamiltonian given in (3.48). The Coloumb interaction $V = 1.7$, the Rabi frequency $\Omega_0 = 0.1$, the laser detuning $\Delta_0 = 1.7$ and the Lamb-Dicke parameter for both qubits $\eta_1 = \eta_2 = 0.1$.

Similarly, we can define the state at a time t being acted on by the actual gate modelled in (3.48) as

$$|t\rangle = \frac{1}{2}[|ss\rangle + |sg\rangle + |gs\rangle + e^{-i\phi_t(t)}|gg\rangle \otimes \sum_{m,n=0}^{N} \mathcal{C}_{mn}(t)|mn\rangle], \qquad (4.13)$$

where $\phi_{ent}(t)$ is the entangled phase as defined above and $\mathcal{C}_{mn}(t)$ is the probability coefficient of the phonon state $|mn\rangle$, both at a given time t.

Now we can derive a new equation for the fidelity of the gate, using (4.9), which gives the result

41

$$F = |\langle \psi_o | t \rangle|^2,$$

$$F = |\frac{1}{4}[\langle ss|ss \rangle + \langle sg|sg \rangle + \langle gs|gs \rangle + e^{i(\phi_{ent}(t)-\pi)} \langle gg|gg \rangle \sum_{m,n=0}^{N} \mathcal{C}_{mn}^{(o)\star} \mathcal{C}_{mn}(t) \langle mn|mn \rangle]|^2,$$

$$F = |\frac{1}{4}[3 + \sum_{m,n=0}^{N} \mathcal{C}_{mn}^{(o)\star} \mathcal{C}_{mn}(t)]|^2,$$

$$F = \frac{1}{16}[3 + \sum_{m,n=0}^{N} \mathcal{C}_{mn}^{(o)\star} \mathcal{C}_{mn}(t)]^2, \tag{4.14}$$

where all parameters are the same as defined previously.

4.3.2 Robust Gate Fidelity from Ideal Initial State

Fig. 4.12 shows the fidelity of the gate modelled by (3.48), using the equation for fidelity in (4.14), for the initial Fock state $|gg, 00\rangle$. We see a very similar, smooth Gaussian curve as in Fig. 4.9. The difference comes in the depth and width of the troughs. For this new method of calculating the fidelity, the minimum value is $F = 0.45$, and the half-depth width of the trough is $225.2(\mu s)/t_f$; for the simple method in section 4.2.3, the minimum value is $F = 0.48$ and the half-depth width is $217.1 \mu s/t_f$.
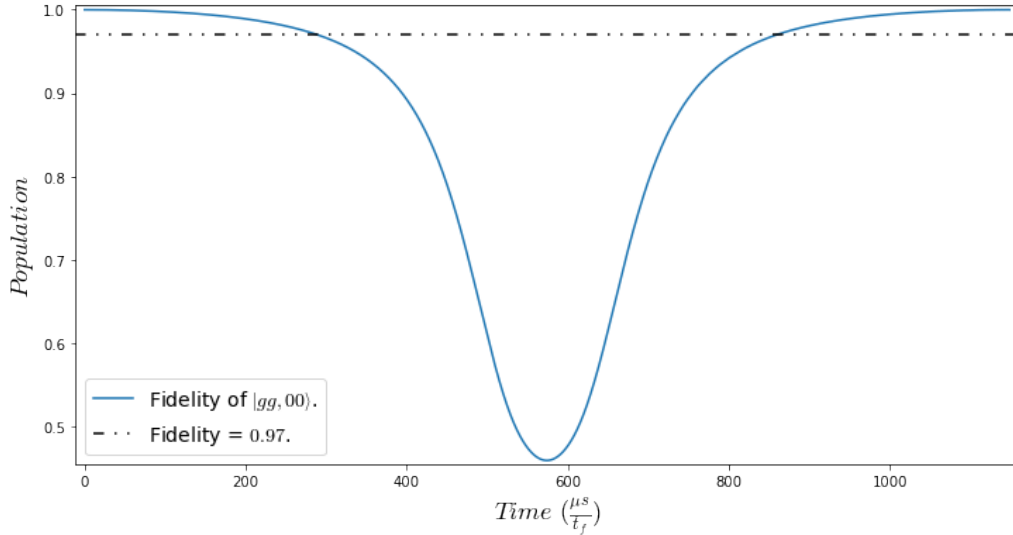
Figure 4.12: The fidelity of the gate through time, calculated using (4.14), for the ideal initial state $|gg, 00\rangle$. The parameters for the Hamiltonian (3.48) used for the gate operation are: The Coloumb interaction $V = 1.7$, the Rabi frequency $\Omega_0 = 0.1$, the laser detuning $\Delta_0 = 1.7$ and the Lamb-Dicke parameter for both qubits $\eta_1 = \eta_2 = 0.1$. As expected, the fidelity of the gate starts, and returns to unity. The dashed horizontal line shows the minimum fidelity required for a scalable quantum computer.

Moreover, a gate fidelity of approximately 0.9999 has been given as the minimum value for scalable quantum computing [22], after reassessment of earlier models. The final fidelity of the gate, shown in Fig. 4.12, is 0.9999472, which meets the scalability requirement. This may not tell the whole story however, as what is shown in Fig. 4.12 is known as the *intrinsic fidelity* [22], i.e. the fidelity of the Hamiltonian modelling the gate, under the perfect conditions of a simulation. In reality, there could be infidelities potentially caused by environmental factors.

4.3.3 Robust Gate Fidelity from Coherent Initial State

Figure 4.13: The fidelity of the gate, through time, for coherent initial states $|gg, \alpha_n \alpha_n\rangle$, where $\alpha_1 = 0.2$, $\alpha_2 = 0.5$ a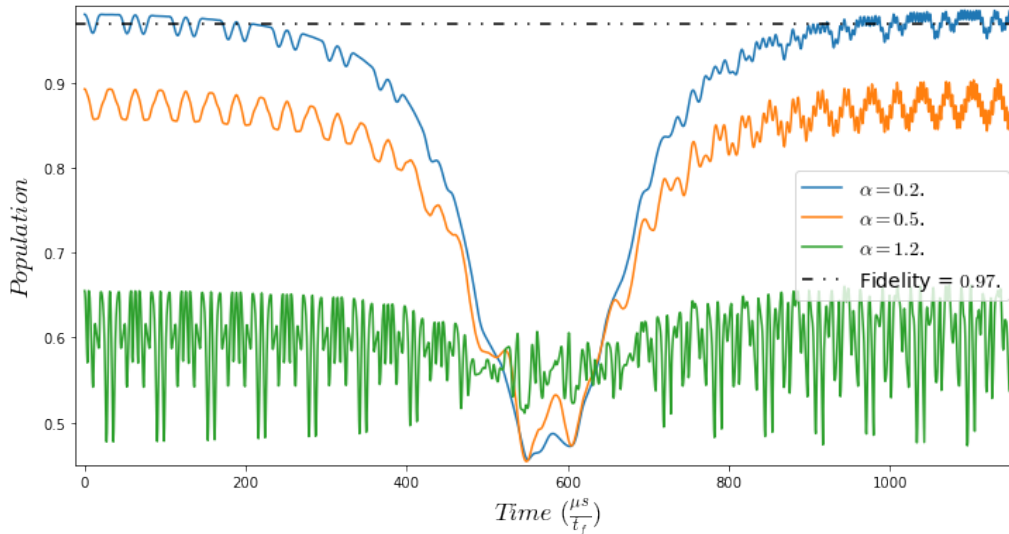nd $\alpha_3 = 1.2$. The parameters for the Hamiltonian (3.48) used for the gate operation are: The Coloumb interaction $V = 1.7$, the Rabi frequency $\Omega_0 = 0.1$, the laser detuning $\Delta_0 = 1.7$ and the Lamb-Dicke parameter for both qubits $\eta_1 = \eta_2 = 0.1$. For all values of α, the oscillations are completely regular before the region of the Gaussian, but become noisy after this region.

Shown in Fig. 4.13 are the fidelities through time for various coherent states, when $\alpha = 0.2, 0.5$ and 1.2. It can be seen that the initial fidelity is no longer unity, as with the simple definition, but it decreases as α increases. This is because as α increases, the initial state $|gg, \alpha\alpha\rangle$ becomes less and less similar to the Fock state $|gg, 00\rangle$. It is also important to note that the fidelity will never be higher than its initial value at $t = 0$. This means that the maximum value of α that could possibly give an acceptable end fidelity is the wherein the fidelity at $t = 0$ is 0.97. This value is $\alpha = 0.25$. Similarly, we can determine the maximum value for α that will result in an end fidelity that satisfies the requirement for a scalable gate of $F = 0.9999$ is $\alpha_{\max} = 0.0525$.

Chapter 5

Conclusion

In summary, the history of quantum computing was introduced in the first two chapters. Focusing on the use of trapped atoms and ions, the development of quantum computing was briefly explored in the second chapter; considering the pros and cons of each proposal, an argument was made for the use of trapped Rydberg ions in quantum computing gates. Chapter three derived and examined the properties of the Jaynes-Cummings model, the mathematical basis of quantum computing using trapped particles.

Finally, in the forth chapter, the Fock state $|gg, 00\rangle$ and coherent states $|gg, \alpha\alpha\rangle$ were analysed for a Hamiltonian modelling the behaviour of MW-dressed Rydberg ions in a linear trap, showing that the gate is capable of achieving fidelities over the threshold of 0.9999 in both cases; the former achieving a fidelity of 0.9999472, the latter having the limit $\alpha_{\max} = 0.0525$ to maintain a fidelity over the threshold. A more realistic model of noise to explore would be thermal states, and following on from that, thermal coherent states [55], which displace thermal states in phase space. The statistical nature of this model may be needed to more accurately simulate the conditions of many gates, as research moves from single gates to multiple. We also know that displacing qubits in phase space has been used as a method to entangle qubits [30], which could reveal a possibility of using thermal coherent states to develop even quicker gates.

References

[1] Juan I Cirac and Peter Zoller. Quantum computations with cold trapped ions. *Physical review letters*, 74(20):4091, 1995.

[2] J Murray-Krezan. The classical dynamics of rydberg stark atoms in momentum space. *American Journal of Physics*, 76(11):1007–1011, 2008.

[3] Weibin Li and Igor Lesanovsky. Entangling quantum gate in trapped ions via rydberg blockade. *Applied Physics B*, 114(1):37–44, 2014.

[4] Alan M Turing. Proposal for development in the mathematics division of an automatic computing engine (ace). *Carpenter, BE, Doran, RW (eds)*, 46, 1986.

[5] Sanjeev Arora and Boaz Barak. Complexity theory: A modern approach, 2009.

[6] Joe P Buhler, Hendrik W Lenstra, and Carl Pomerance. Factoring integers with the number field sieve. In *The development of the number field sieve*, pages 50–94. Springer, 1993.

[7] Steven George Krantz. *The proof is in the pudding: The changing nature of mathematical proof.* Springer, 2011.

[8] Oded Goldreich and Avi Wigderson. Iv. 20 computational complexity. In *The Princeton Companion to Mathematics*, pages 575–604. Princeton University Press, 2010.

[9] Paul Adrien Maurice Dirac. *The principles of quantum mechanics.* Number 27. Oxford university press, 1981.

[10] Peter W Shor. Algorithms for quantum computation: discrete logarithms and factoring. In *Proceedings 35th annual symposium on foundations of computer science*, pages 124–134. Ieee, 1994.

[11] David Beckman, Amalavoyal N Chari, Srikrishna Devabhaktuni, and John Preskill. Efficient networks for quantum factoring. *Physical Review A*, 54(2):1034, 1996.

[12] Jacob Biamonte, Peter Wittek, Nicola Pancotti, Patrick Rebentrost, Nathan Wiebe, and Seth Lloyd. Quantum machine learning. *Nature*, 549(7671):195–202, 2017.

[13] AV Frolov. Can a quantum computer be applied for numerical weather prediction? *Russian meteorology and hydrology*, 42(9):545–553, 2017.

[14] John Clarke and Frank K Wilhelm. Superconducting quantum bits. *Nature*, 453(7198):1031–1042, 2008.

[15] William M Kaminsky, Seth Lloyd, and Terry P Orlando. Scalable superconducting architecture for adiabatic quantum computation. *arXiv preprint quant-ph/0403090*, 2004.

[16] Emanuel Knill, Raymond Laflamme, and Gerald J Milburn. A scheme for efficient quantum computation with linear optics. *nature*, 409(6816):46–52, 2001.

[17] Anders Sørensen and Klaus Mølmer. Quantum computation with ions in thermal motion. *Physical review letters*, 82(9):1971, 1999.

[18] Jan Benhelm, Gerhard Kirchmair, Christian F Roos, and Rainer Blatt. Towards fault-tolerant quantum computing with trapped ions. *Nature Physics*, 4(6):463–466, 2008.

[19] TP Harty, DTC Allcock, C J Ballance, L Guidoni, HA Janacek, NM Linke, DN Stacey, and DM Lucas. High-fidelity preparation, gates, memory, and readout of a trapped-ion quantum bit. *Physical review letters*, 113(22):220501, 2014.

[20] Chi Zhang, Fabian Pokorny, Weibin Li, Gerard Higgins, Andreas Pöschl, Igor Lesanovsky, and Markus Hennrich. Submicrosecond entangling gate between trapped ions via rydberg interaction. *Nature*, 580(7803):345–349, 2020.

[21] Cheng Sheng, Xiaodong He, Ruijun Guo, Kunpeng Wang, Peng Xu, Zongyuan Xiong, Min Liu, Jin Wang, and Mingsheng Zhan. High fidelity single-qubit gates of a single neutral atom in the magic-intensity optical dipole trap. *arXiv preprint arXiv:1712.06306*, 2017.

[22] Mark Saffman. Quantum computing with atomic qubits and rydberg interactions: progress and challenges. *Journal of Physics B: Atomic, Molecular and Optical Physics*, 49(20):19, 2016.

[23] Simon J Devitt, William J Munro, and Kae Nemoto. Quantum error correction for beginners. *Reports on Progress in Physics*, 76(7):076001, 2013.

[24] Mark Saffman, Thad G Walker, and Klaus Mølmer. Quantum information with rydberg atoms. *Reviews of modern physics*, 82(3):17–18, 2010.

[25] Paul Benioff. The computer as a physical system: A microscopic quantum mechanical hamiltonian model of computers as represented by turing machines. *Journal of statistical physics*, 22(5):563–591, 1980.

[26] Alan Mathison Turing. On computable numbers, with an application to the entscheidungsproblem. a correction. *Proceedings of the London Mathematical Society*, 2(1):544–546, 1938.

[27] Paul Benioff. Quantum mechanical hamiltonian models of turing machines. *Journal of Statistical Physics*, 29(3):515–546, 1982.

[28] David P DiVincenzo. The physical implementation of quantum computation. *Fortschritte der Physik: Progress of Physics*, 48(9-11):771–783, 2000.

[29] Chris Monroe, David M Meekhof, Barry E King, Wayne M Itano, and David J Wineland. Demonstration of a fundamental quantum logic gate. *Physical review letters*, 75(25):4714, 1995.

[30] Dietrich Leibfried, Brian DeMarco, Volker Meyer, David Lucas, Murray Barrett, Joe Britton, Wayne M Itano, B Jelenković, Chris Langer, Till Rosenband, et al. Experimental demonstration of a robust, high-fidelity geometric two ion-qubit phase gate. *Nature*, 422(6930):412–415, 2003.

[31] D Jaksch, JI Cirac, P Zoller, SL Rolston, R Côté, and MD Lukin. Fast quantum gates for neutral atoms. *Physical Review Letters*, 85(10):2208, 2000.

[32] Thad G Walker and Mark Saffman. Entanglement of two atoms using rydberg blockade. *Advances in Atomic, Molecular, and Optical Physics*, 61:81–115, 2012.

[33] L Isenhower, E Urban, XL Zhang, AT Gill, T Henage, Todd A Johnson, TG Walker, and M Saffman. Demonstration of a neutral atom controlled-not quantum gate. *Physical review letters*, 104(1):010503, 2010.

[34] Todd A Johnson, E Urban, T Henage, L Isenhower, DD Yavuz, TG Walker, and M Saffman. Rabi oscillations between ground and rydberg states with dipole-dipole atomic interactions. *Physical Review Letters*, 100(11):113003, 2008.

[35] Igor E Protsenko, Georges Reymond, Nicolas Schlosser, and Philippe Grangier. Operation of a quantum phase gate using neutral atoms in microscopic dipole traps. *Physical Review A*, 65(5):052301, 2002.

[36] M Saffman and TG Walker. Analysis of a quantum logic device based on dipole-dipole interactions of optically trapped rydberg atoms. *Physical Review A*, 72(2):022347, 2005.

[37] Mark Saffman, Thad G Walker, and Klaus Mølmer. Quantum information with rydberg atoms. *Reviews of modern physics*, 82(3):14–15, 2010.

[38] Markus Müller, Linmei Liang, Igor Lesanovsky, and Peter Zoller. Trapped rydberg ions: from spin chains to fast quantum gates. *New Journal of Physics*, 10(9):093009, 2008.

[39] Daniel FV James. Quantum dynamics of cold trapped ions with application to quantum computation. Technical report, 1997.

[40] Paul R Berman and Vladimir S Malinovsky. *Principles of laser spectroscopy and quantum optics*. Princeton University Press, 2010.

[41] John W Negele and Henri Orland. *Quantum many-particle systems*. CRC Press, 2018.

[42] Claude Cohen-Tannoudji, Jacques Dupont-Roc, and Gilbert Grynberg. *Atom-photon interactions: basic processes and applications*. 1998.

[43] Pierre Meystre and Murray Sargent. *Elements of quantum optics*. Springer Science & Business Media, 2007.

[44] David J Wineland, C Monroe, Wayne M Itano, Dietrich Leibfried, Brian E King, and Dawn M Meekhof. Experimental issues in coherent quantum-state manipulation of trapped atomic ions. *Journal of research of the National Institute of Standards and Technology*, 103(3):259, 1998.

[45] Jürgen Eschner, Giovanna Morigi, Ferdinand Schmidt-Kaler, and Rainer Blatt. Laser cooling of trapped ions. *JOSA B*, 20(5):1003–1015, 2003.

[46] Johannes Maximilian Nipper. Interacting rydberg atoms: Coherent control at förster resonances and polar homonuclear molecules. 2012.

[47] Sylvain Ravets, Henning Labuhn, Daniel Barredo, Thierry Lahaye, and Antoine Browaeys. Measurement of the angular dependence of the dipole-dipole interaction between two individual rydberg atoms at a förster resonance. *Physical Review A*, 92(2):020701, 2015.

[48] Adriano Barenco, Charles H Bennett, Richard Cleve, David P DiVincenzo, Norman Margolus, Peter Shor, Tycho Sleator, John A Smolin, and Harald Weinfurter. Elementary gates for quantum computation. *Physical review A*, 52(5):3457–3467, 1995.

[49] Michael A Nielsen and Isaac L Chuang. Quantum computation and information theory, 2010.

[50] Jean-Pierre Gazeau. *Coherent States in Quantum Optics*. Berlin: Wiley-VCH, 2009.

[51] Roy J Glauber. Coherent and incoherent states of the radiation field. *Physical Review*, 131(6):2766, 1963.

[52] Abhishek Shukla, Mitali Sisodia, and Anirban Pathak. Complete characterization of the directly implementable quantum gates used in the ibm quantum processors. *Physics Letters A*, 384(18):126387, 2020.

[53] Easwar Magesan, Robin Blume-Kohout, and Joseph Emerson. Gate fidelity fluctuations and quantum process invariants. *Physical Review A*, 84(1):012309, 2011.

[54] Michael A Nielsen. A simple formula for the average gate fidelity of a quantum dynamical operation. *Physics Letters A*, 303(4):249–252, 2002.

[55] J Oz-Vogt, A Mann, and M Revzen. Thermal coherent states and thermal squeezed states. *Journal of Modern Optics*, 38(12):2339–2347, 1991.